THE JOURNAL OF PHYSICAL CHEMISTRY C

Article

pubs.acs.org/JPCC

Interactions and Inhibition Effect of Urea-Derived Mannich Bases on a Mild Steel Surface in HCl

Mani Jeeva,[†] G. Venkatesa Prabhu,[*,†] Maria susai Boobalan,[‡] and Chinnaiyan Mahalingam Rajesh[§]

[†]Department of Chemistry, National Institute of Technology, Tiruchirappalli-620015, Tamilnadu, India

[‡]Department of Chemistry, St. Joseph's College, Tiruchirapalli-620002, Tamilnadu, India

[§]Department of Chemistry, Indian Institute of Technology, Guwahati-781039, Assam, India

Supporting Information

ABSTRACT: Cost-effective new Mannich bases 1-(pyridin-4-yl(pyrrolidin-1-yl)methyl)urea (UPyP), 1-(morpholino-(pyridin-4-yl)methyl)urea (UMP), and 1-(piperidin-1-yl-(pyridin-4-yl)methyl)urea (UPP) were synthesized, characterized, and examined as corrosion inhibitors for the corrosion of a mild steel surface in 1.0 M hydrochloric acid (HCl) solution using weight loss, potentiodynamic polarization, and electrochemical impedance spectroscopy (EIS) measurements. The X-ray structures of UMP and UPP are reported. The inhibition efficiency increases with increasing inhibitor concentration and decreases with increasing solution temperature. Potentiodynamic polarization measurements showed that all inhibitors are mixed type. The values of thermodynamic and activation parameters were calculated and discussed. Adsorption of inhibitors on the mild steel surface in the presence of HCl follows Langmuir's adsorption isotherm. The relationship between molecular structure and their inhibition efficiencies has been studied using density functional theory (DFT) calculations. Experimental and theoretical results are in good agreement.

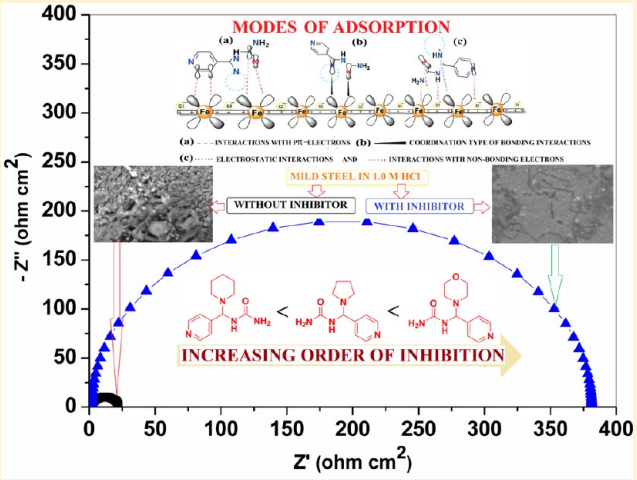

1. INTRODUCTION

Mild steel is one of the important materials used in various industries due to its excellent mechanical properties and low cost. Hydrochloric acid solution is widely used in many industrial processes such as removal of rust in metal finishing industries, cleaning of boilers, steel pickling, acid descaling, oil well acidizing, ore processing, recovery of ion exchangers, and petroleum processes.[1−4] However, during such processes the components of the metal structure are damaged due to the aggressiveness of hydrochloric acid.[4,5] Hence, inhibitors are commonly used in these processes to reduce excessive metal dissolution and to minimize the consumption of acid.[4−6] Corrosion inhibitors have been classified as organic and inorganic inhibitors.[7] Use of inorganic inhibitors such as chromates, dichromate, molybdate, tetraborate, arsenates, and phosphates is mostly avoided due to their biotoxicity, presence of heavy metals, and environmental hazardness.[8] When using inorganic inhibitors, maintaining pH of solution and concentration of inhibitors is very critical. The most effective way is to use nontoxic organic inhibitors instead of using inorganic inhibitors for anticorrosion.

Most of the well-known inhibitors are organic compounds containing multiple bonds and heteroatoms like N, O, and S, which can donate lone pair electrons, found to be very efficient as inhibitors against metal corrosion in many environments.[9−12] Nitrogen-based heterocyclic compounds are effective inhibitors for mild steel corrosion in acidic solution.[12,13] According to this, Mannich bases act as corrosion inhibitors due to the presence of π-electrons of the aromatic ring and larger number of heteroatoms, which adsorb onto the metal surface through nonbonded electron pairs on the heteroatom. This induces greater adsorption of the compounds and decreases the corrosion rate.[13−17] The degree of adsorption of inhibitor molecules on the mild steel surface is influenced by molecular size, geometrical shape and steric factor, orientation of the electron donor site in acid medium, and thermal stability of the inhibitor.[18−20]

The study of Mannich bases attracted a great deal of attention from chemists because it plays a vital role owing to their wide range of pharmacological and industrial applications, and they have several biological activities such as cytotoxic, local anesthetics, antihypertensive, antimalarial, antitubercular, antioxidant, and antibacterial activities. Other applications are in agro chemicals such as plant growth regulators, cross-linking agents, ion exchangers, flocculants, surfactants, flame retardants, and corrosion inhibitors.[21−24]

Received: June 17, 2015
Revised: August 21, 2015
Published: September 6, 2015

DOI: 10.1021/acs.jpcc.5b05788
J. Phys. Chem. C 2015, 119, 22025−22043

Presently, quantum chemical calculations and molecular simulation studies have been proved to be a very useful tool for studying the mechanism of corrosion inhibition.[18,25−27] The quantum chemical parameters such as energy of molecular orbitals, highest occupied molecular orbital (HOMO) and lowest unoccupied molecular orbital (LUMO), energy gap (ΔE) between HOMO and LUMO, dipole moment, electronic chemical potential (μ), chemical hardness (η), electron affinity (EA), ionization potential (IP), and number of transferable electrons from inhibitor to the metal surface (ΔN) are directly related to the performance of inhibitors.[28−30]

The aim of the present work is to investigate the inhibition properties of newly synthesized 1-(pyridin-4-yl(pyrrolidin-1-yl)methyl)urea (UPyP), 1-(morpholino(pyridin-4-yl)methyl)-urea (UMP), and 1-(piperidin-1-yl(pyridin-4-yl)methyl)urea (UPP) on the corrosion behavior of mild steel in 1.0 M HCl solution using gravimetric (weight loss), electrochemical, and computational methods.[18,31] These selective inhibitors are synthesized appropriately from relatively very cheap starting materials. The electronic structure properties such as frontier molecular orbital (FMO) analysis, Mulliken atomic charge analysis, and molecular electrostatic potential (MEP) analysis were carried out to understand the efficiency of inhibitors toward corrosion inhibition.

2. EXPERIMENTAL SECTION

2.1. Materials and Methods. Mild steel samples having an elemental composition of (wt %) 0.14% C, 0.35% Mn, 0.17% Si, 0.025% S, 0.03% P, and balance Fe were used for weight loss, electrochemical studies, as well as SEM analysis. The samples were cut to dimensions of 5.0 cm × 2.0 cm × 0.2 cm, and the surface was polished using 1/0, 2/0, 3/0, and 4/0 grade emery papers and finally washed with acetone and double distilled water, dried at room temperature, and immediately used for experiments. The aggressive solutions were made of HCl 37% (Merck). The solution of 1.0 M HCl was prepared by using double distilled water. The concentrations of the used inhibitors ranged from 30 to 200 ppm in 1.0 M HCl for all the experiments.

All the reagents and solvents used for synthesizing the inhibitors were of Analar grade (Merck) and were used as such without further purification. Melting points were determined in an open capillary tube with a VEEGO VMP-CM melting point apparatus. The microelemental analysis was carried out with a Carlo Erba 1108 Elemental Analyzer. The purity of the compounds was checked by thin-layer chromatography (TLC). FT-IR spectra were recorded on a PerkinElmer IR spectrophotometer. Both ^{1}H NMR and ^{13}C NMR spectra were recorded on a Bruker spectrometer employing TMS as the internal reference and DMSO-d_6 as solvent at ambient temperature. UV−visible spectra were recorded in methanol on a EZ301 PerkinElmer spectrophotometer. High-resolution mass spectra were recorded on an Agilent 6500 (ESI-MS) Q-TOP mass spectrometer.

2.2. Synthesis of Mannich Bases. Inhibitor compounds (UPyP, UMP, and UPP) were synthesized according to the general procedure described in the literature (Figure 1).[21,32−34] A homogeneous ethanolic solution of urea (1.8 g, 0.03 mol) and appropriate secondary aliphatic amine (0.03 mol) was prepared.

To this mixture pyridine 4-carboxaldehyde (3.0 mL, 0.03 mol) was added in drops with constant stirring. The contents were stirred at 65 °C until the solution become oily. After cooling to RT, a solid mass was obtained, and it was washed with double distilled water several times and dried in the air oven at 75 °C.

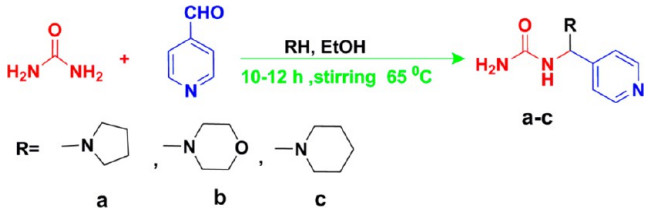

Figure 1. Scheme for synthesis of Mannich bases: (a) UPyP, (b) UMP, and (c) UPP.

1-(Pyridin-4-yl(pyrrolidin-1-yl)methyl)urea (UPyP). Pale brown solid (79% yield); mp 114−115 °C. Anal. Calcd for $C_{11}H_{16}N_4O$: C, 59.98; H, 7.32; N, 25.44%. Found: C, 59.82; H, 7.27; N, 25.47%. ^{1}H NMR (400 MHz, DMSO-d_6): δ (ppm) 1.66 (s, 4H, CH_2 pyrrolidine-3′&4′), 2.43 (d, 4H, J = 9.2 Hz, N−CH_2 pyrrolidine-2′&5′), 5.48 (d, 1H, J = 9.2 Hz, NH), 5.63 (s, 2H, NH_2), 6.85 (d, 1H, J = 9.2 Hz, CH), 7.35 (d, 2H, J = 4.0 Hz, $ArH_{3,5}$), 8.53 (d, 2H, J = 4.0 Hz, $ArH_{2,6}$). ^{13}C{^{1}H} NMR (100 MHz, DMSO-d_6): δ (ppm) 23.3, 48.2, 68.2, 122.3, 149.8, 150.7, 158.6. FT-IR (KBr, cm^{-1}): $\overline{\nu}_{max}$ 588, 687, 775, 1119, 1141, 1206, 1460, 1548, 1602, 1658, 2879, 2934, 3084, 3196, 3295, 3450. HRMS: calcd for $C_{11}H_{16}N_4O$: $[M]^+$ 220.1324; found $[M]^+$ 220.1329.

1-(Morpholino(pyridin-4-yl)methyl)urea (UMP). White solid (88% yield); mp 156−157 °C. Anal. Calcd for $C_{11}H_{16}N_4O_2$: C, 55.92; H, 6.83; N, 23.71%. Found: C, 55.87; H, 6.79; N, 23.75%. ^{1}H NMR (300 MHz, DMSO-d_6): δ (ppm) 2.37 (s, 4H, N−CH_2 morpholine), 3.56−3.59 (m, 4H, O−CH_2 morpholine), 5.46 (d, 1H, J = 9.9 Hz, NH), 5.71 (s, 2H, NH_2), 6.85 (d, 1H, J = 9.9 Hz, CH), 7.38 (d, 2H, J = 5.4 Hz, $ArH_{3,5}$), 8.55 (d, 2H, J = 5.4 Hz, $ArH_{2,6}$). ^{13}C{^{1}H} NMR (75 MHz, DMSO-d_6): δ (ppm) 48.1, 66.2, 70.4, 122.3, 149.2, 149.6, 158.4. FT-IR (KBr, cm^{-1}): $\overline{\nu}_{max}$ 592, 681, 789, 1068, 1112, 1130, 1193, 1460, 1539, 1602, 1630, 1665, 2857, 2955, 3132, 3311, 3395. HRMS: calcd for $C_{11}H_{16}N_4O_2$: $[M]^+$ 236.1273; found $[M]^+$ 236.1266.

1-(Piperidin-1-yl(pyridin-4-yl)methyl)urea (UPP). White solid (88% yield); mp 159−160 °C. Anal. Calcd for $C_{12}H_{18}N_4O$: C, 61.52; H, 7.74; N, 23.91%. Found: C, 61.49; H, 7.87; N, 23.77%. ^{1}H NMR (400 MHz, DMSO-d_6): δ (ppm) 1.41−1.45 (m, 2H, CH_2 piperidine-4′), 1.51−1.59 (m, 4H, CH_2 piperidine-3′&5′), 2.45 (s, 4H, N−CH_2 piperidine-2′&6′), 2.73 (s, 2H, NH_2), 5.20 (s, 1H, NH), 5.62 (d, 1H, J = 8.8 Hz, CH), 7.41 (d, 2H, J = 5.2 Hz, $ArH_{3,5}$), 8.57 (d, 2H, J = 5.2 Hz, $ArH_{2,6}$). ^{13}C{^{1}H} NMR (100 MHz, DMSO-d_6): δ (ppm) 29.2, 30.8, 44.8, 53.8, 76.2, 127.2, 154.3, 154.4, 164.3. FT-IR (KBr, cm^{-1}): $\overline{\nu}_{max}$ 579, 681, 779, 1113, 1150, 1195, 1439, 1538, 1603, 1659, 1676, 2848, 2936, 3055, 3171, 3276, 3415. HRMS: calcd for $C_{12}H_{18}N_4O$: $[M]^+$ 234.1481; found $[M]^+$ 234.1487.

2.3. X-ray Crystallography. Selected single crystals were used for collection of intensity data on a SuperNova (single source at offset), Eos diffractometer with graphite monochromated Mo Kα radiation (λ = 0.71073 Å) using CrysAlisPro, Agilent Technologies, Version 1.171.36.20 data collection software. Single crystals were fixed onto the tip of the glass fiber using Quickfix for the X-ray data collection. The collection method involved phi and omega scans. The crystal structure was solved by direct methods using SHELXTL.[35] Non-hydrogen atoms were first refined isotropically followed by anisotropic refinement by full matrix least-squares calculations based on F^2 using SHELXTL. Hydrogen atoms were first located in the difference map then positioned geometrically and allowed to ride on their respective parent atoms. Hydrogen atoms involved in

DOI: 10.1021/acs.jpcc.5b05788
J. Phys. Chem. C 2015, 119, 22025−22043

Table 1. Crystal Data and Structure Refinement for UMP and UPP

abbreviation	UMP	UPP
CCDC No.	994959	967686
empirical formula	$C_{11}H_{16}N_4O_2$	$C_{12}H_{18}N_4O$
formula weight	236.27	234.30
temperature (K)	293(2)	296(2)
wavelength (Å)	0.71073	0.71073
crystal system	orthorhombic	orthorhombic
space group	*Fdd*2	*Fdd*2
crystal size (mm^3)	1.0 × 0.8 × 0.6	0.3 × 0.20 × 0.15
a (Å)	12.2079(11)	12.6630(17)
b (Å)	34.449(3)	33.528(4)
c (Å)	11.8236(6)	12.2027(12)
α (deg)	90	90
volume ($Å^3$)	4972.4(7)	5180.8(11)
Z	1	16
calculated density (g/cm^3)	1.262	1.202
absorption coefficient (mm^{-1})	0.090	0.080
F(000)	2016	2016
θ range for data collection (deg)	2.98−28.80	2.95−28.53
limiting indices	$-15 \le h \le 15, -45 \le k \le 43, -15 \le l \le 14$	$-9 \le h \le 16, -42 \le k \le 41, -16 \le l \le 8$
reflections collected	12059	3393
unique reflections (R_{int})	2984 (0.0223)	2014 (0.0309)
absorption correction	multiscan	none
max. and min transmission	0.917 and 0.947	0.9881 and 0.9763
refinement method	full-matrix least-squares on F^2	full-matrix least-squares on F^2
data/restraints/parameters	2984/1/154	2014/1/159
goodness-of-fit on F^2 (S)	0.818	1.063
final R_2, wR_2[a] (observed data)	$R_1 = 0.0450$, $wR_2 = 0.1677$	$R_1 = 0.0533$, $wR_2 = 0.1345$
final R_2, wR_2[a] (all data)	$R_1 = 0.0546$, $wR_2 = 0.1969$	$R_1 = 0.0705$, $wR_2 = 0.1543$
absolute structure parameter	1.8(18)	−3(2)
largest different in peak and hole ($e.Å^{-3}$)	0.127, −0.153	0.179, −0.156

[a] $R_1 = \sum||F_0| - |F_c||/\sum|F_0|$ and $wR_2 = [\sum(w(F_0^2 - F_c^2)^2)/\sum(w(F_0^2)^2]^{(1/2)}$ where *w* is the Chebychew polynomial with 3 parameters 8.3157, 1.5359, 6.3603.

hydrogen bonding were located in the difference map and refined freely. Diagrams and publication material were generated using SHELXTL, WinGX,[36] and ORTEP-3.[37] Crystal data and structure refinement for compounds UMP and UPP are summarized in Table 1.

2.4. Weight Loss Measurements. Weight loss measurements were carried out by weighing the mild steel specimens before and after immersion in 100 mL of 1.0 M HCl containing different concentrations of the studied inhibitors for 2 h at various temperatures. The weight loss of the specimens was determined using an analytical balance accurate to 0.01 mg. All experiments were performed under the atmospheric ambient, and the temperature of the solutions was controlled by thermostat. Duplicate experiments were performed in each case, and the mean results were taken.

The inhibition efficiency (IE %) and surface coverage (θ) were determined by using the following equation.[38]

$$\text{IE}\ (\%) = \frac{(W_0 - W_i)}{W_0} \times 100 \quad (1)$$

$$\theta = \frac{(W_0 - W_i)}{W_0} \quad (2)$$

where W_0 and W_i are the values of the weight loss without and with addition of the inhibitor, respectively.

The corrosion rate (C_R) of mild steel was calculated using the following expression.[9]

$$C_R = \frac{(W_0 - W_i)}{A \times T} \quad (3)$$

where *A* is the area of the mild steel specimen (cm^2) and *T* is the exposure time (h).

Weight loss measurements were repeated at different temperatures from 305 to 335 K in the absence and presence of different inhibitor concentrations, to determine the effect of temperature on the inhibition efficiency of studied inhibitors.

2.5. Electrochemical Measurements. All the electrochemical measurements were performed using the Electrochemical Workstation (CH electrochemical analyzer model 604B, USA), and a constant temperature of 32 ± 0.5 °C is maintained with 1.0 M HCl as the electrolyte. A platinum electrode and a saturated calomel electrode (SCE) were used as counter and reference electrodes, respectively, while the working electrode was comprised of mild steel specimens of 1.0 cm^2 exposed area. To obtain the steady state, the mild steel specimens were immersed for 30 min in 100 mL of 1.0 M HCl solution containing various concentrations of inhibitors before Tafel polarization and EIS measurements. After 30 min immersion, the open-circuit potential (OCP) was recorded as a function of time for 300 s. Figure 2 shows the steady-state OCP curves for a mild steel specimen in 1.0 M HCl solution containing different concentrations of inhibitors.[9] Tafel curves were obtained by changing the electrode potential automatically from −250 to +250 mV versus OCP at a scan rate of 10 mV s^{-1}. The percentage

DOI: 10.1021/acs.jpcc.5b05788
J. Phys. Chem. C 2015, 119, 22025−22043

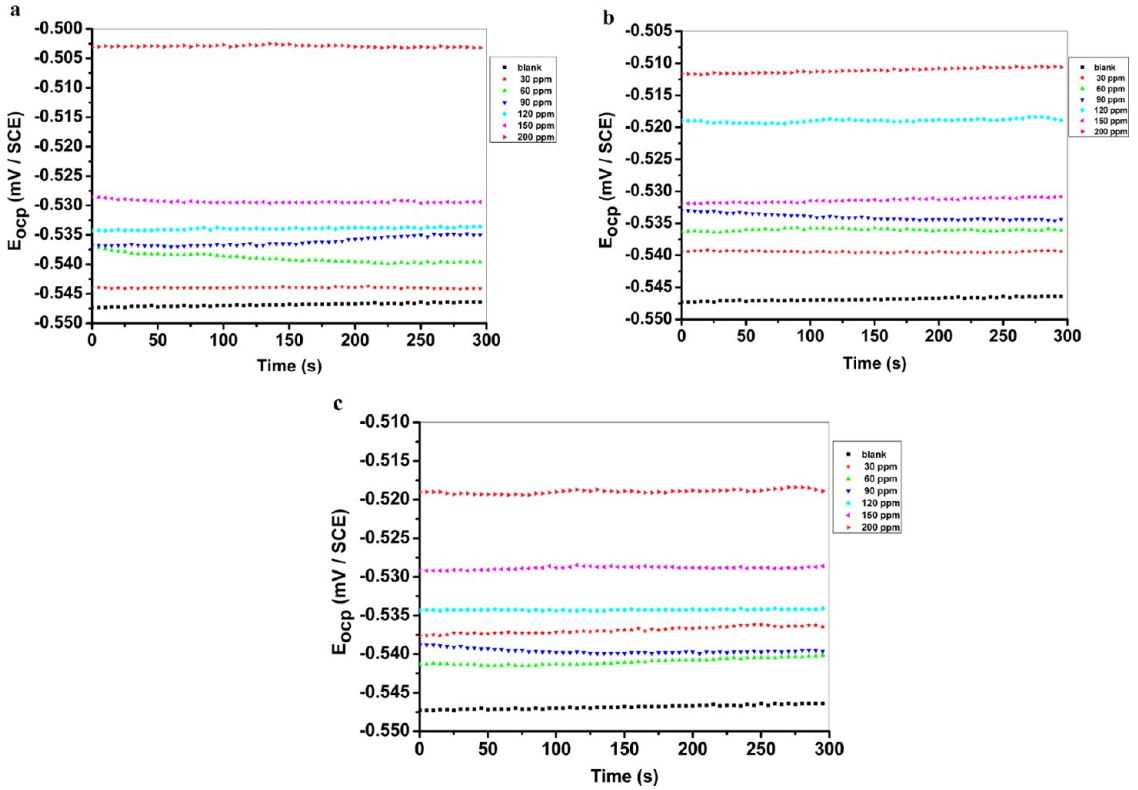

Figure 2. Variation of open-circuit potential with time for mild steel in 1.0 M HCl solution containing different concentrations of (a) UPyP, (b) UMP, and (c) UPP at 305 K.

inhibition efficiency (IE, %) from potentiodynamic polarization was calculated by using the following equation.[19]

$$\mathrm{IE}\ (\%) = \frac{(I_0 - I')}{I_0} \times 100 \tag{4}$$

where I_0 and I' are the corrosion current density without and with the inhibitor, respectively.

Impedance measurements were carried out in the frequency range from 0.1 to 10000 Hz at the open-circuit potential, by applying 0.01 V sine wave AC voltage. The impedance diagrams are given by Nyquist representation. The percentage inhibition efficiency (IE, %) was calculated from the charge-transfer resistance values according to the equation[4]

$$\mathrm{IE}\ (\%) = \frac{(R_{CT} - R'_{CT})}{R_{CT}} \times 100 \tag{5}$$

where R_{CT} and R'_{CT} are charge transfer resistance in the presence and absence of inhibitor, respectively.

Double-layer capacitance (C_{dl}) was determined from the following relation[38]

$$C_{dl} = \frac{1}{2\pi f_{max} R_{CT}} \tag{6}$$

where f_{max} is the frequency at maximum imaginary component (Z'_{max}) of the impedance.

2.6. SEM Analysis. The surface morphology of each specimen after immersion in 100 mL of 1.0 M HCl in the absence and presence of inhibitors was studied using a VEGA3 TESCAN scanning electron microscope at CARE, Tiruchirappalli, Tamilnadu, India. The working sample was analyzed at different locations to ensure reproducibility.

2.7. Quantum Chemical Analysis. The molecular structure of the inhibitor takes the prominent responsibility in the prevention of corrosion progression upon the surface of a metal. An exclusive comprehension can be archived when the experimental results are combined and interpreted with theoretical calculations by means of certain attributes on anticorrosion treatment.[39] Those attributes are calculated by using quantum chemical methods such as E_{HOMO}, E_{LUMO}, ΔE, i.e., energy gap between HOMO and LUMO, Mullikan charges, dipole moment, electronic chemical potential (μ), chemical hardness (η), electron affinity (EA), ionization potential (IP), global electrophilicity index (ω), and number of transferable electrons from inhibitor to metal surface (ΔN).[3,40]

The theoretical and physical understanding of these quantum chemical descriptors can aid one to gain superior chemical insight toward the structure−function relation of reported Mannich bases. Generally, the mathematical foundation for μ and η originated from HSAB principle and was based on first and second partial derivatives of ground-state molecular energy E against electron number N, at constant peripheral potential ν.[11,40]

$$\mu = \left(\frac{\partial E}{\partial N}\right)_{\nu(r)} \tag{7}$$

$$\eta = \frac{1}{2}\left(\frac{\partial^2 E}{\partial N^2}\right)_{\nu(r)} \tag{8}$$

The ground-state parabola model[41] of these equations can be given by

$$\mu = -\frac{I + A}{2} \tag{9}$$

DOI: 10.1021/acs.jpcc.5b05788
J. Phys. Chem. C 2015, 119, 22025−22043

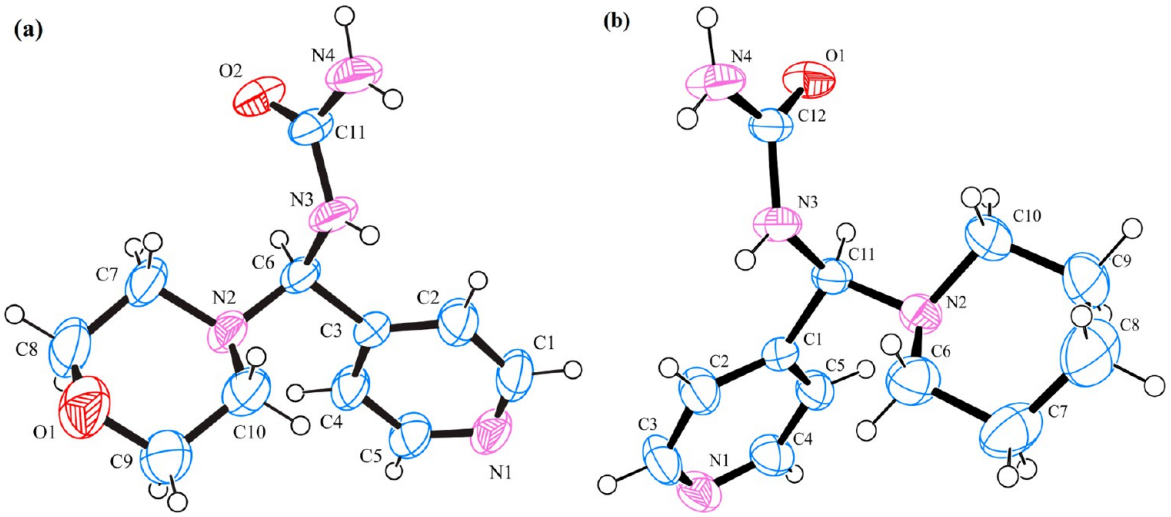

Figure 3. Molecular structures with the atom numbering scheme of (a) UMP and (b) UPP, showing 40% probability displacement ellipsoids.

Table 2. Inhibition Efficiency Obtained by Weight Loss of Mild Steel in 1.0 M HCl Containing Various Concentrations of Mannich Base Inhibitors at Different Temperatures

		UPyP			UMP			UPP		
temp. (K)	inhibitor conc.	C_R (mg cm^{-2} h^{-1})	IE (%)	θ	C_R (mg cm^{-2} h^{-1})	IE (%)	θ	C_R (mg cm^{-2} h^{-1})	IE (%)	θ
305	blank	1.95	-	-	1.95	-	-	1.95	-	-
	30	0.83	57.8	0.578	0.80	59.1	0.591	0.84	57.1	0.571
	60	0.73	62.3	0.623	0.66	66.2	0.662	0.7	64.0	0.640
	90	0.58	70.5	0.705	0.55	71.8	0.718	0.58	70.1	0.701
	120	0.49	75.0	0.750	0.42	78.2	0.782	0.47	75.6	0.756
	150	0.35	82.1	0.821	0.31	84.1	0.841	0.4	77.9	0.779
	200	0.26	86.7	0.867	0.23	88.3	0.883	0.27	86.0	0.860
315	blank	2.41	-	-	2.41	-	-	2.41	-	-
	30	1.16	52.0	0.520	1.11	54.1	0.541	1.19	50.7	0.507
	60	1.06	56.2	0.562	0.97	59.6	0.596	1.04	56.7	0.567
	90	0.89	63.3	0.633	0.80	66.9	0.669	0.9	62.7	0.627
	120	0.72	70.3	0.703	0.63	74.0	0.740	0.73	69.8	0.698
	150	0.59	75.3	0.753	0.51	79.0	0.790	0.58	75.9	0.759
	200	0.44	81.9	0.819	0.37	84.5	0.845	0.44	81.6	0.816
325	blank	3.03	-	-	3.03	-	-	3.03	-	-
	30	1.60	47.1	0.471	1.51	50.0	0.500	1.63	46.2	0.462
	60	1.34	55.6	0.556	1.34	55.6	0.556	1.42	53.1	0.531
	90	1.25	58.6	0.586	1.16	61.5	0.615	1.23	59.2	0.592
	120	1.02	66.3	0.663	0.94	68.8	0.688	1.08	64.4	0.644
	150	0.84	72.4	0.724	0.78	74.3	0.743	0.92	69.5	0.695
	200	0.73	75.7	0.757	0.65	78.5	0.785	0.75	75.1	0.751
335	blank	3.53	-	-	3.53	-	-	3.53	-	-
	30	1.94	45.2	0.452	1.96	44.4	0.444	2.01	43.0	0.430
	60	1.79	49.3	0.493	1.76	50.2	0.502	1.89	46.4	0.464
	90	1.61	54.5	0.545	1.55	56.1	0.561	1.65	53.4	0.534
	120	1.41	60.0	0.600	1.3	63.1	0.631	1.44	59.3	0.593
	150	1.19	66.3	0.663	1.13	68.1	0.681	1.22	65.4	0.654
	200	1.04	70.6	0.706	0.94	73.3	0.733	1.09	69.2	0.692

$$\eta = \frac{I - A}{2} \tag{10}$$

where I and A represent vertical ionization potential (IP) and electron affinity (EA) accordingly. The global electrophilicity index (ω)[42] can be expressed by

$$\omega = \frac{\chi^2}{2\eta} = \frac{E^2_{\mathrm{HOMO}} + 2E_{\mathrm{HOMO}}E_{\mathrm{LUMO}} + E^2_{\mathrm{LUMO}}}{4(E_{\mathrm{LUMO}} - E_{\mathrm{HOMO}})} \tag{11}$$

where χ is recognized as Mulliken electronegativity and related[43] as $\mu = -\chi$.

According to Sanderson's principle of electronegativity equalization[44] and Lukovit's observation,[45] the electron transfer from inhibitor to metal surface has been represented by ΔN and mathematically given as

$$\Delta N = \frac{\chi_{\mathrm{Fe}} - \chi_{\mathrm{inhibitor}}}{2(\eta_{\mathrm{Fe}} + \eta_{\mathrm{inhibitor}})} \tag{12}$$

DOI: 10.1021/acs.jpcc.5b05788
J. Phys. Chem. C 2015, 119, 22025−22043

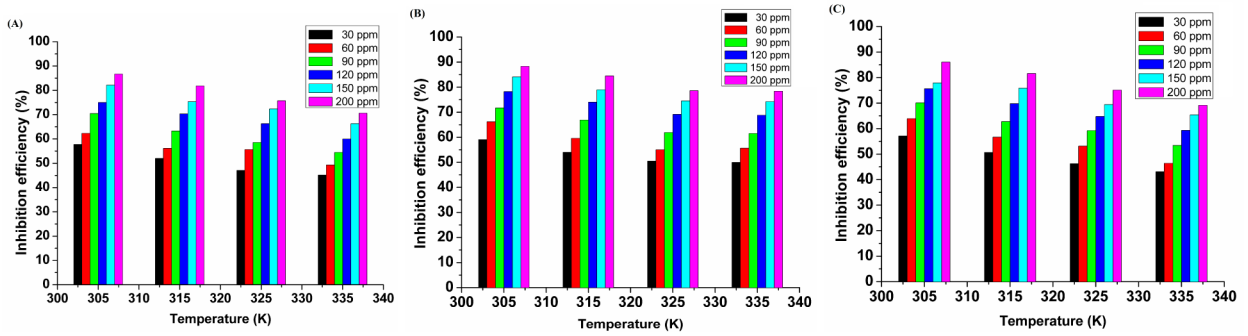

Figure 4. Variation of inhibition efficiencies of (A) UPyP, (B) UMP, and (C) UPP at different temperatures.

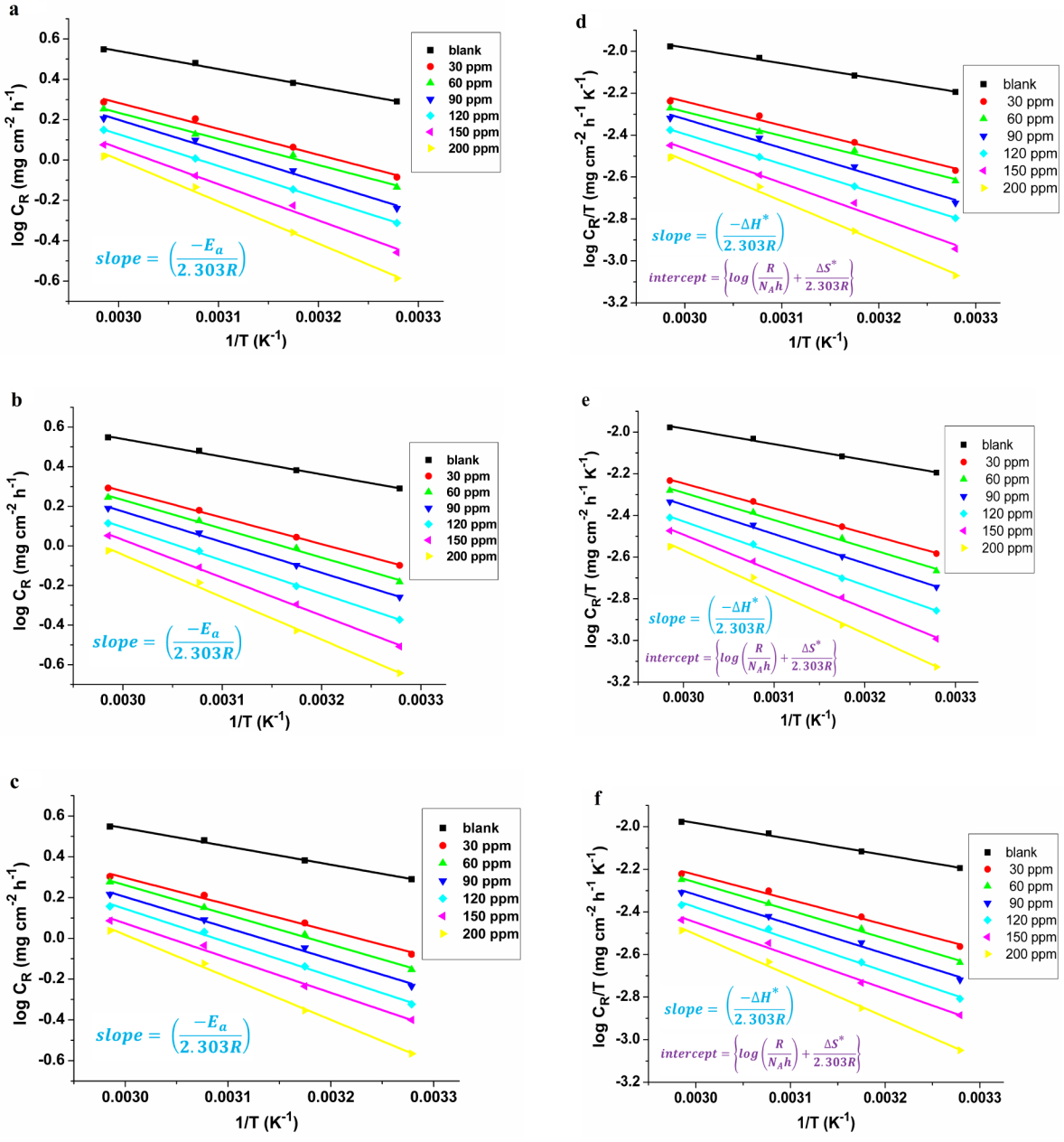

Figure 5. Arrhenius (a. UPyP, b. UMP, and c. UPP) and Eyring (d. UPyP, e. UMP, and f. UPP) plots for corrosion of mild steel in 1.0 M HCl containing various concentrations of Mannich base inhibitors.

The entire calculations were performed using the Gaussian03 package under B3LYP/6-31G(d,p) level model chemistry to compute the above said properties, which have a pivotal role in determining inhibition competence.[46]

DOI: 10.1021/acs.jpcc.5b05788
J. Phys. Chem. C 2015, 119, 22025−22043

Table 3. Activation Parameters for Corrosion of Mild Steel in 1.0 M HCl Containing Various Concentrations of Mannich Base Inhibitors at Different Temperatures

inhibitor	conc. (ppm)	E_a (kJ mol^{-1})	A (mg cm^{-2} h^{-1})	ΔH^*_{corr} (kJ mol^{-1})	$-\Delta S^*_{corr}$ (J mol^{-1}K^{-1})
none	blank	17.10	1.66×10^3	14.42	192.30
UPyP	30	24.65	1.40×10^4	21.95	174.62
	60	24.80	1.32×10^4	22.10	175.11
	90	29.20	5.95×10^4	26.49	162.60
	120	30.14	7.68×10^4	27.43	161.16
	150	34.30	2.71×10^5	31.59	150.00
	200	39.83	1.75×10^6	37.11	134.53
UMP	30	25.63	1.96×10^4	22.93	171.81
	60	27.84	3.92×10^4	25.13	166.05
	90	29.65	6.59×10^4	26.94	161.74
	120	32.13	1.34×10^5	29.42	155.82
	150	36.59	5.80×10^5	33.87	143.69
	200	41.00	2.39×10^6	38.27	131.94
UPP	30	25.14	1.72×10^4	22.44	172.89
	60	27.91	4.30×10^4	25.20	165.29
	90	29.25	6.10×10^4	26.54	162.38
	120	31.62	1.25×10^5	28.91	156.41
	150	32.59	1.51×10^5	29.88	154.86
	200	39.90	1.85×10^6	37.17	134.05

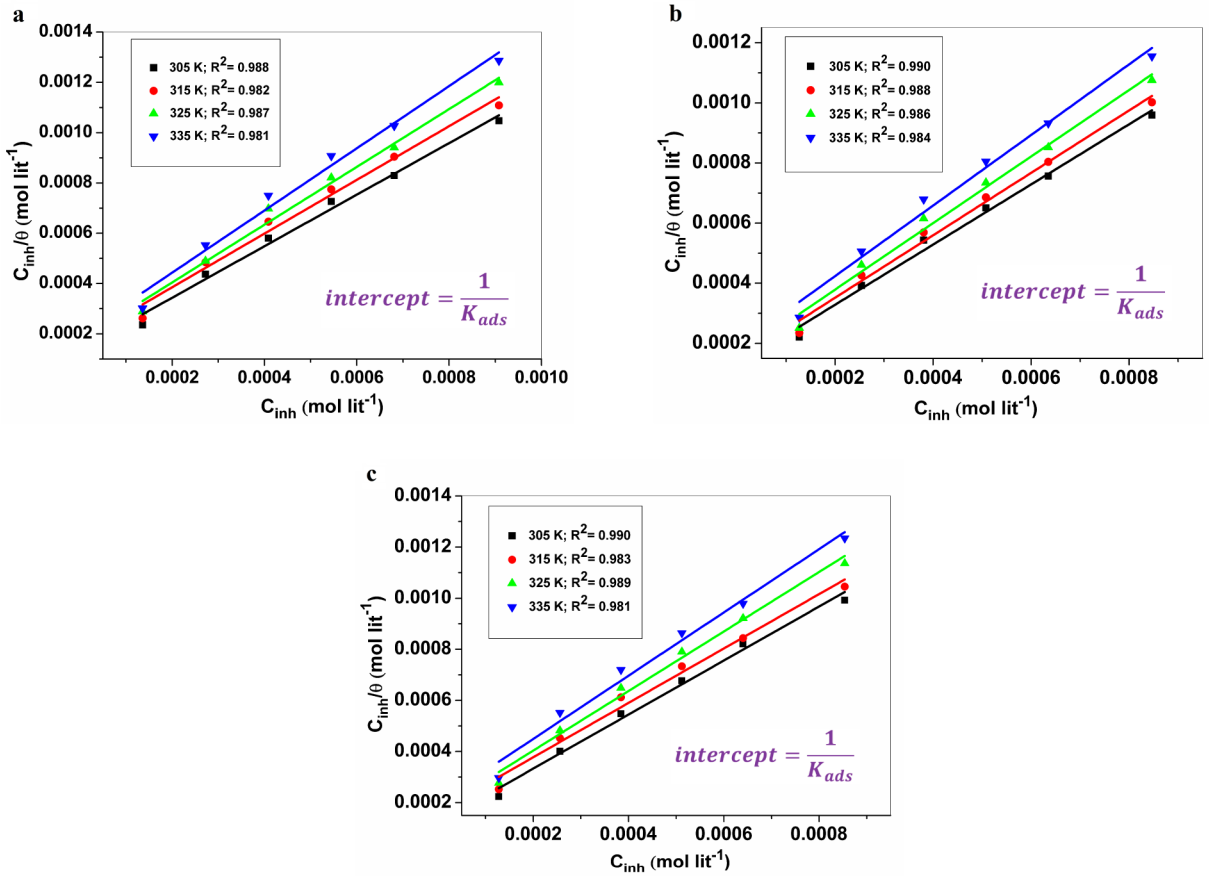

Figure 6. Langmuir isotherm plots for mild steel in 1.0 M HCl solution containing different concentration of (a) UPyP, (b) UMP, and (c) UPP at different temperatures.

3. RESULTS AND DISCUSSION

3.1. Characterization of Inhibitors. The Mannich bases (UPyP, UMP, and UPP) were synthesized from the reactions of urea with three different secondary aliphatic amines (pyrrolidine, morpholine, and piperidine) and pyridine 4-carboxaldehyde in ethanol under stirring at 65 °C for 10−12 h. The yield of the reactions and melting points of the compounds were determined, and the structures of Mannich bases were characterized by elemental analysis, FT-IR, ^{1}H and ^{13}C NMR, and ESI-mass spectroscopy.

DOI: 10.1021/acs.jpcc.5b05788
J. Phys. Chem. C 2015, 119, 22025−22043

Table 4. Thermodynamic Parameters for Adsorption of Inhibitors in 1.0 M HCl on the Steel Surface at Different Temperatures

inhibitor	temp. (K)	K_{ads} (L mol^{-1})	$-\Delta G^0_{ads}$ (kJ mol^{-1})	$-\Delta H^0_{ads}$ (kJ mol^{-1})	ΔS^0_{ads} (J mol^{-1} K^{-1})	$-\Delta H^0_{ads}$ [a] (kJ mol^{-1})	ΔS^0_{ads} [a] (J mol^{-1} K^{-1})
UPyP	305	7228	32.73	9.019	77.72	8.968	77.60
	315	5833	33.24	9.019	76.88	-	-
	325	5736	34.25	9.019	77.62	-	-
	335	5109	34.98	9.019	77.49	-	-
UMP	305	7800	32.92	10.572	73.26	10.6605	73.10
	315	6949	33.69	10.572	73.40	-	-
	325	6360	34.52	10.572	73.70	-	-
	335	5294	35.08	10.572	73.14	-	-
UPP	305	8226	33.05	13.233	64.98	13.0705	65.10
	315	6083	33.35	13.233	63.85	-	-
	325	5864	34.31	13.233	64.84	-	-
	335	4963	34.90	13.233	64.67	-	-

[a]Values are obtained from verification plot of ΔG^0_{ads} versus T.

Table 5. Polarization Parameter and Inhibition Efficiency of Mild Steel in 1.0 M HCl Containing Various Concentrations of Mannich Base Inhibitors at 305 K

inhibitor	conc. (ppm by weight)	I_{corr} (μA cm^{-2})	$-E_{corr}$ (mV vs SCE)	β_a (mV/Decade)	$-\beta_c$ (mV/Decade)	θ	IE (%)
none	blank	923.50	553	103	186	-	-
UPy4P	30	207.80	517	76	171	0.775	77.50
	60	158.90	521	69	192	0.828	82.79
	90	118.60	514	94	127	0.872	87.16
	120	92.22	502	64	110	0.900	90.01
	150	49.47	529	72	128	0.946	94.64
	200	35.47	508	47	153	0.962	96.16
UM4P	30	194.10	533	62	182	0.790	78.98
	60	156.00	501	67	110	0.831	83.11
	90	109.90	532	69	192	0.881	88.10
	120	89.76	513	63	184	0.903	90.28
	150	48.85	548	95	121	0.947	94.71
	200	29.88	510	45	145	0.968	96.76
UP4P	30	229.00	521	94	189	0.752	75.20
	60	174.20	539	74	166	0.811	81.14
	90	128.60	518	69	209	0.861	86.07
	120	98.70	528	93	137	0.893	89.31
	150	79.13	506	62	170	0.914	91.43
	200	47.25	466	49	110	0.949	94.88

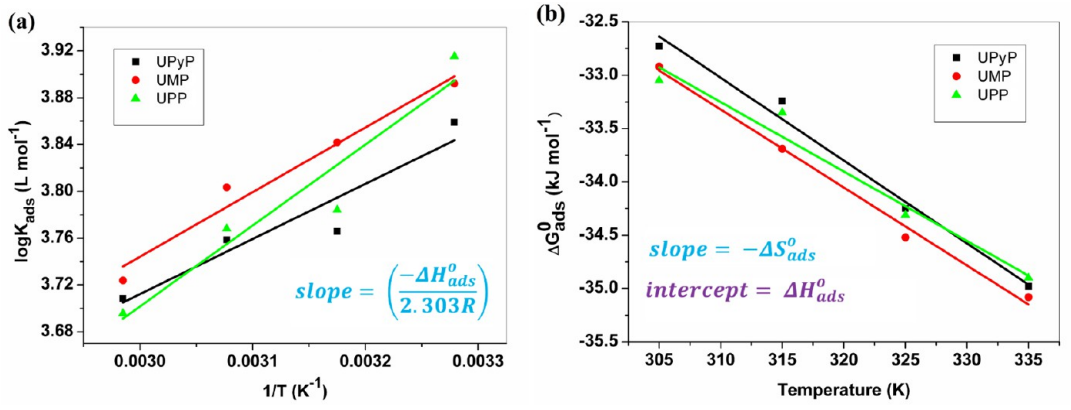

Figure 7. (a) Linear regression between log K_{ads} and $1/T$ and (b) verification plot of ΔG^0_{ads} versus T.

The FT-IR spectra of the Mannich bases show characteristic bands due to the ν(C═O), ν(C═C), ν(C−N), ν(C−H), and ν(N−H) functional groups. The secondary aliphatic amine ν(C−N−C) stretching vibrations of UPyP, UMP, and UPP occur at 1141, 1130, and 1152 cm^{-1}, respectively. The distinct absorption band occurs at 1112−1119 cm^{-1} assigned for newly formed ν(C−N−C) stretching frequency. This favorably indicates the substitution on urea and aliphatic amines and confirms the formation of new Mannich bases.

The ^{1}H and ^{13}C NMR spectra further confirmed the anticipated structures. The ^{1}H NMR data for the compounds in DMSO-d_6 show the two doublets observed at δ 7.4 and 8.5

DOI: 10.1021/acs.jpcc.5b05788
J. Phys. Chem. C 2015, 119, 22025−22043

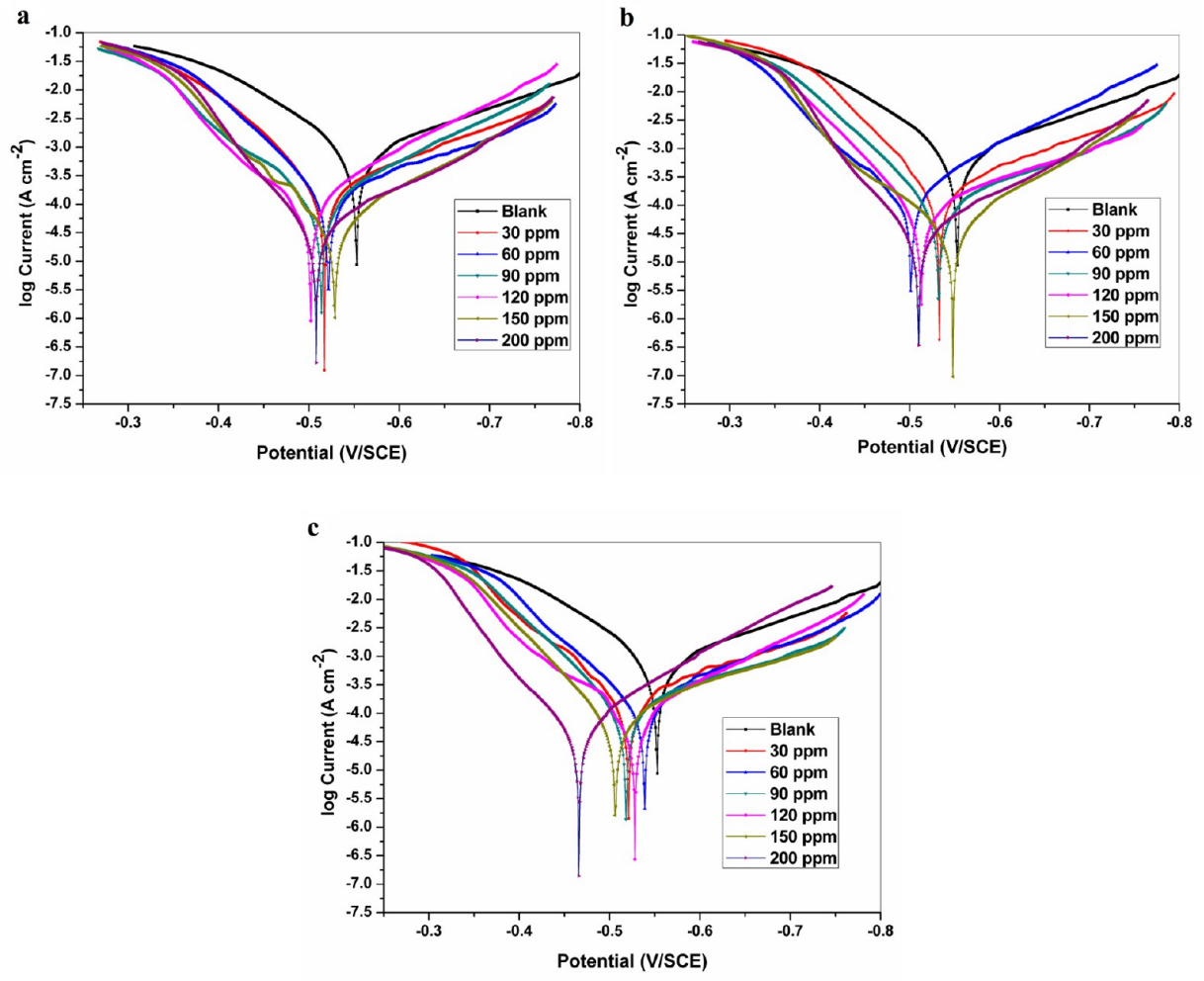

Figure 8. Anodic and cathodic Tafel lines for mild steel in uninhibited 1.0 M HCl and with different concentrations of inhibitors: (a) UPyP, (b) UMP, and (c) UPP.

ppm are attributed to the protons of the 4-pyridinyl ring. The signal of the methine CH proton of UPyP, UMP, and UPP is observed at δ 6.85, 6.85, and 5.62 ppm, respectively, which indicates the formation of a new compound. All expected resonances were observed in the ^{13}C NMR spectra of compounds. The signal for the carbonyl carbon of urea present in UPyP, UMP, and UPP appears at δ 158.6, 158.4, and 164.3 ppm, respectively. The high-resolution mass spectra confirm the assigned molecular mass of the compounds.

3.2. X-ray Crystallography Studies. Good quality crystals suitable for single-crystal X-ray diffraction analyses were obtained for compounds UMP and UPP. Both UMP and UPP were crystallized in the space group of *Fdd*2 in the orthorhombic crystal system. The compounds UMP and UPP contain two ring systems, viz., the 4-pyridinyl ring and the morpholino/piperidinyl ring which are linked through the urea moiety. The molecular structures with the atom numbering scheme of UMP and UPP are shown in Figure 3.

3.3. Corrosion Inhibition Studies. *3.3.1. Weight Loss Method. 3.3.1.1. Effect of Inhibitor Concentration.* The weight loss data of the mild steel samples in 1.0 M HCl with various concentrations of inhibitors (30−200 ppm by weight) and without inhibitors at different temperatures (305−335 K) are listed in Table 2. From the data, the corrosion inhibition efficiency for all synthesized inhibitors increases with increasing inhibitor concentrations. Even though experiments were conducted at higher concentrations of inhibitors (i.e., 250 and 300 ppm), there was no remarkable increase in the inhibition efficiency since 200 ppm was found to be the optimal concentration.

3.3.1.2. Effect of Solution Temperature and Activation Parameters of the Corrosion Process. In order to investigate the effect of temperature on the corrosion process of mild steel in 1.0 M HCl solution, the weight loss experiments were performed at 10 K intervals in the temperature range of 305−335 K in the presence and absence of different concentrations of inhibitors during 2 h immersion.[38] The effect of solution temperature on inhibition efficiencies is shown in Figure 4. It was found that the inhibition efficiency decreases with increase in solution temperature 305−335 K. This may be due to desorption of the inhibitor molecules from the mild steel surface at elevated temperatures.[3,13]

A correlation between the corrosion rate (C_R) and absolute temperature (T) can be expressed by the Arrhenius equation.[1,3]

$$C_R = A \exp\left(\frac{-E_a}{RT}\right) \tag{13}$$

where E_a is apparent activation energy; A is the pre-exponential factor; and R is the universal gas constant.

DOI: 10.1021/acs.jpcc.5b05788
J. Phys. Chem. C 2015, 119, 22025−22043

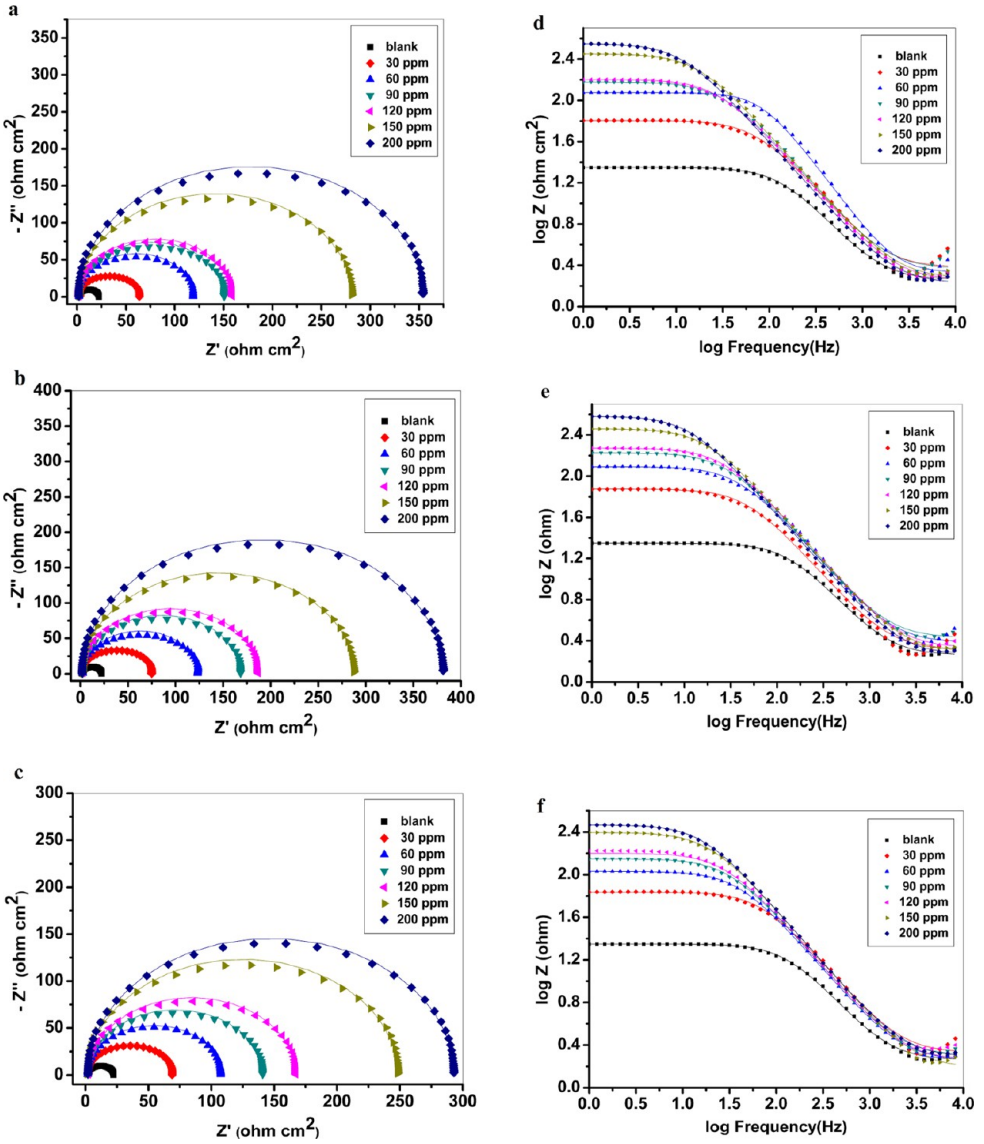

Figure 9. Nyquist (a. UPyP, b. UMP, and c. UPP) and Bode (d. UPyP, e. UMP, and f. UPP) plots of EIS measurements of mild steel in uninhibited 1.0 M HCl and with different concentrations of inhibitors (characteristic symbols and solid lines show experimental and fitted results, respectively).

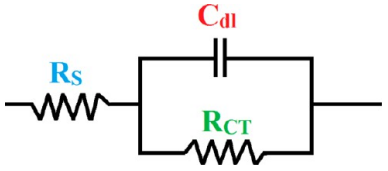

Figure 10. Equivalent circuit model used to fit the Nyquist plots shown in Figures 9 (R_S = solution resistance, R_{CT} = charge-transfer resistance ($R_{CT} = R_f + R_d + R_a$), and C_{dl} = double layer capacitance).

A plot of log of corrosion rate obtained by weight loss measurement versus $1/T$ gave a straight line as shown in Figure 5 for mild steel in 1.0 M HCl in the presence of different concentrations of inhibitors (a) UPyP, (b) UMP, and (c) UPP. The values of activation energy E_a obtained from the slope ($-E_a/2.303R$) of the straight lines are given in Table 3. The values of E_a for the corrosion of mild steel in 1.0 M HCl in the presence of inhibitors are higher than in the absence of the inhibitors. It can be seen in Table 3 that the activation energy increases with concentration of inhibitor, and consequently the rate of corrosion decreases.

The apparent enthalpy of activation ΔH^*_{corr} and the apparent entropy of activation ΔS^*_{corr} can be obtained from the Eyring transition state equation.[15,28]

$$C_R = \frac{RT}{N_A h} \exp\left(\frac{\Delta S^*_{corr}}{R}\right) \exp\left(\frac{-\Delta H^*_{corr}}{RT}\right) \quad (14)$$

where h is Planck's constant and N_A the Avogadro number. Figure 4 shows plots of $\log(C_R/T)$ versus $1/T$ obtained for mild steel in 1.0 M HCl without and with the presence of different concentrations of Mannich base inhibitors gave straight lines with slope $-\Delta H^*_{corr}/2.303R$ and intercept $[\log(R/N_A h) + \Delta S^*_{corr}/2.303R]$. The calculated values of ΔH^*_{corr} and ΔS^*_{corr} obtained from these plots are given in Table 3. The values of change in activation entropy, ΔS^*_{corr}, in the presence of the inhibitor are large and negative indicating that the activated complex in the rate-determining step is associative in nature, and therefore, the activated complex has more orderly structure.[28] At the same time the values of ΔS^*_{corr}slightly increase with the

DOI: 10.1021/acs.jpcc.5b05788
J. Phys. Chem. C 2015, 119, 22025−22043

Table 6. Electrochemical Impedance Parameters and Inhibition Efficiency of Mild Steel in 1.0 M HCl Containing Various Concentrations of Mannich Base Inhibitors at 305 K

		experimental data				simulation data			
inhibitor	concentration (ppm by weight)	R_{CT} (Ω cm^2)	f_{max}	C_{dl} (μF cm^{-2})	IE (%)	R_{CT} (Ω cm^2)	f_{max}	C_{dl} (μF cm^{-2})	IE (%)
none	blank	20.54	9.72	797.20	-	20.46	10.18	764.13	-
UPyP	30	61.77	27.87	92.45	66.75	61.25	30.58	84.95	66.61
	60	116.82	60.56	22.50	82.42	116.80	58.50	22.50	82.49
	90	148.30	67.88	15.81	86.15	148.00	73.60	13.06	86.18
	120	156.91	74.28	13.66	86.91	157.00	78.31	11.02	86.97
	150	279.18	132.30	4.31	92.64	279.20	138.80	4.56	92.68
	200	352.72	166.30	2.71	94.18	352.30	175.60	2.39	94.20
UMP	30	72.96	33.15	65.81	71.85	72.72	36.30	60.29	71.86
	60	121.00	54.40	24.18	83.03	120.90	60.27	21.84	83.08
	90	165.35	77.50	12.42	87.58	165.60	82.06	11.71	87.64
	120	184.75	87.39	9.86	88.88	184.40	92.00	9.38	88.90
	150	285.10	137.80	4.05	92.80	285.40	142.40	3.92	92.83
	200	379.80	182.30	2.30	94.59	379.60	189.10	2.22	94.61
UPP	30	67.09	30.81	70.80	69.38	66.81	33.90	64.56	69.38
	60	105.88	50.90	25.84	80.60	105.70	52.43	25.11	80.64
	90	138.72	65.79	14.63	85.19	138.80	68.89	13.95	85.26
	120	165.35	78.07	11.04	87.58	164.90	81.55	10.58	87.59
	150	247.16	117.10	4.77	91.69	246.80	122.30	4.56	91.71
	200	291.68	139.30	3.01	92.96	291.0	144.60	2.90	92.97

concentrations of inhibitors which suggests that the availability of corrosion reaction sites is random and decreases with inhibitor concentration.[47]

The positive values of ΔH^*_{corr} in both the absence and presence of inhibitor reflect the endothermic nature of the mild steel dissolution process suggesting that the dissolution of steel is slow in the presence of inhibitors.[1,47] It is also clear that the values of E_a and ΔH^*_{corr} enhanced with the inhibitor concentration suggest that the energy barrier of corrosion reaction increases with the presence of Mannich base inhibitors. Consequently, the corrosion reaction will be hindered at the metal surface sites.

3.3.1.4. Adsorption Isotherm and Thermodynamic Parameters. The selection of organic inhibitor molecules is based on their ability to interact with the metal surface in acidic medium. The adsorption of organic inhibitor molecules at the metal/solution interface may take place through the polar amine group present in the inhibitor, which displaces the adsorbed water molecules at the metal surface. This displacement reaction can be given by the reaction scheme[48]

$$\mathrm{Org}_{soln} + x\mathrm{H_2O}_{ads} \leftrightarrow \mathrm{Org}_{ads} + x\mathrm{H_2O}_{soln} \quad (15)$$

where x is the number of water molecules displaced by one molecule of organic inhibitor. Basic information on the interaction between the inhibitor and the mild steel surface can be provided by the adsorption isotherm. The most frequently used adsorption isotherms are Langmuir, Temkin, and Frumkin. The Langmuir adsorption isotherm was found to be the best fit for a organic compound in hydrochloric acid solution. The linear regression fitting to the Langmuir adsorption isotherm is illustrated by plotting C_{inh}/θ versus C_{inh} (Figure 6) according to the following equation[29]

$$\frac{C_{inh}}{\theta} = \frac{1}{K_{ads}} + C_{inh} \quad (16)$$

where K_{ads} is the adsorption equilibrium constant and C_{inh} is the concentration of inhibitor. The strong correlation ($R^2 > 0.98$) suggests that the adsorption of the inhibitor on the mild steel surface obeyed this isotherm and well agrees with experimental data. Then K_{ads} values can be calculated from the slopes of straight lines which are given in Table 4. It is a known fact that K_{ads} represents the strength between adsorbate and adsorbent. Large values of K_{ads} indicate that the inhibitor is strongly adsorbed on the metal surface and hence has better inhibition efficiency.[3] In addition, the values of K_{ads} decrease with increasing solution temperature due to thermal agitation of inhibitor molecules.

The values of free energy of adsorption (ΔG^0_{ads}) are calculated using the following equation and are listed in Table 4.

$$\Delta G^0_{ads} = -RT \ln(55.5K_{ads}) \quad (17)$$

where 55.5 is the molar concentration of water in the solution expressed in M (mol L^{-1}); T is the absolute temperature (K); and R is the gas constant (8.314 J K^{-1} mol^{-1}). The negative values of ΔG^0_{ads} (Table 5) ensure the spontaneity of the adsorption process and stability of the adsorbed layer on the steel surface. The ΔG^0_{ads} values range between −32 and −35 kJ mol^{-1}, which are lower than −20 kJ mol^{-1} (Table 4); this specifies that the adsorption of inhibitor molecules on the mild steel surface involves both physisorption and chemisorption.[3,14]

According to the Van't Hoff equation, the standard adsorption enthalpy (ΔH^0_{ads}) can be calculated by linear regression between $\log K_{ads}$ and $1/T$ (Figure 7a), and the results are shown in Table 4.

$$\log K_{ads} = \frac{-\Delta H^0_{ads}}{2.303RT} + \text{constant} \quad (18)$$

The values of the standard entropy of adsorption (ΔS^0_{ads}) were obtained from the thermodynamic basic equation, and the values of ΔH^0_{ads} and ΔS^0_{ads} were evaluated from the slope and the intercept of the plot of ΔG^0_{ads} versus T (Figure 7b). The values of ΔH^0_{ads} and ΔS^0_{ads} were calculated and listed in Table 4.

$$\Delta G^0_{ads} = \Delta H^0_{ads} - T\Delta S^0_{ads} \quad (19)$$

DOI: 10.1021/acs.jpcc.5b05788
J. Phys. Chem. C 2015, 119, 22025−22043

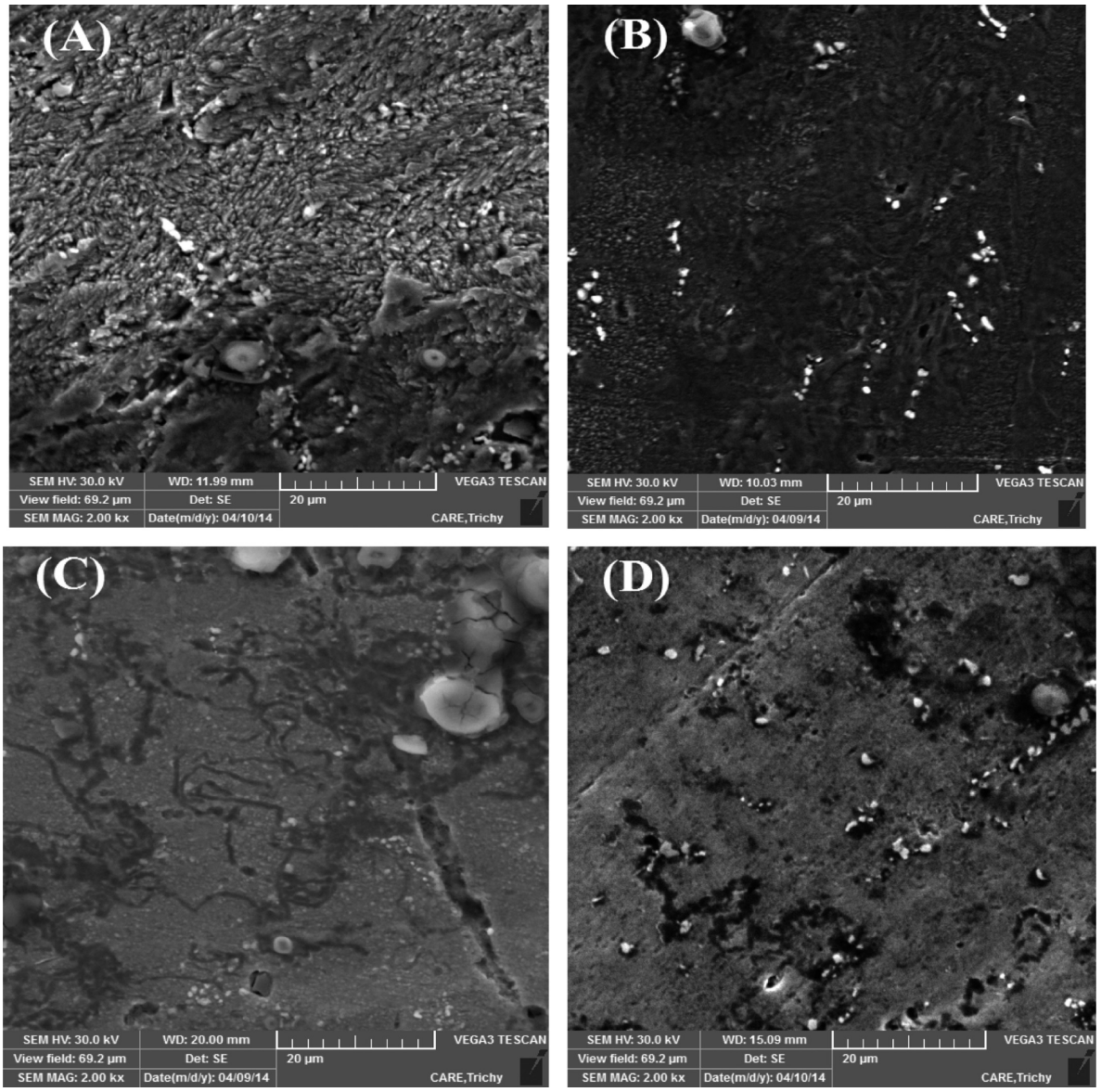

Figure 11. SEM micrographs (× 2000) of the surface of mild steel after 5 h of immersion in 1.0 M HCl: (A) without inhibitor; (B) in the presence of 200 ppm of UPyP; (C) in the presence of 200 ppm of UMP; and (D) in the presence of 200 ppm of UPP.

The values of the enthalpy of adsorption (ΔH^0_{ads}) obtained from both eq 18 and eq 19 are in good agreement. The negative values of ΔH^0_{ads} illustrate that the adsorption of inhibitor on a mild steel surface is an exothermic process.[49] Generally, an exothermic process signifies either physisorption or chemisorption, while the endothermic process is attributed to chemisorption. In an exothermic process, physisorption is distinguished from chemisorption by considering the absolute enthalpy value of a physisorption process which is lower than −40 kJ mol^{-1}, while the adsorption heat of a chemisorption process approaches −100 kJ mol^{-1}.[50] In the present study, the values of standard adsorption heat ranging between −9 and −13 kJ mol^{-1} show that a comprehensive adsorption (physical adsorption) might occur. The ΔS^0_{ads} values in the presence of inhibitor are positive, which illustrate that desorption of water molecules takes place from the metal/solution interface during adsorption of organic inhibitor on the steel surface.[29]

3.2. Tafel Polarization Studies. Figure 8 shows the cathodic and anodic polarization curves of mild steel in 1.0 M HCl in the absence and presence of different concentration of inhibitors UPyP, UMP, and UPP at 305 K, respectively. The electrochemical corrosion kinetic parameters such as corrosion potential (E_{corr}), cathodic and anodic Tafel slops (β_c, β_a), and corrosion current density (I_{corr}), obtained by extrapolation of Tafel lines, are listed in Table 5. The data show the I_{corr} values decrease considerably in the presence of inhibitors and decreased with increasing inhibitor concentration showing increased inhibition efficiency. The decrease in I_{corr} with increasing inhibitor concentration was associated with the shift of corrosion potential, E_{corr}, to a less negative value. This indicates that all the inhibitors suppressed the anodic reaction (hydrogen evolution reaction) to greater extents than the cathodic one, at all concentrations. Also, this suggests that the adsorbed inhibitors might form a surface film that acts as a physical barrier to control the diffusion of ions from the mild steel surface and consequently retard the corrosion process.

3.3. Electrochemical Impedance Spectroscopy. The corrosion behavior of mild steel in 1.0 M HCl in the absence and

DOI: 10.1021/acs.jpcc.5b05788
J. Phys. Chem. C 2015, 119, 22025−22043

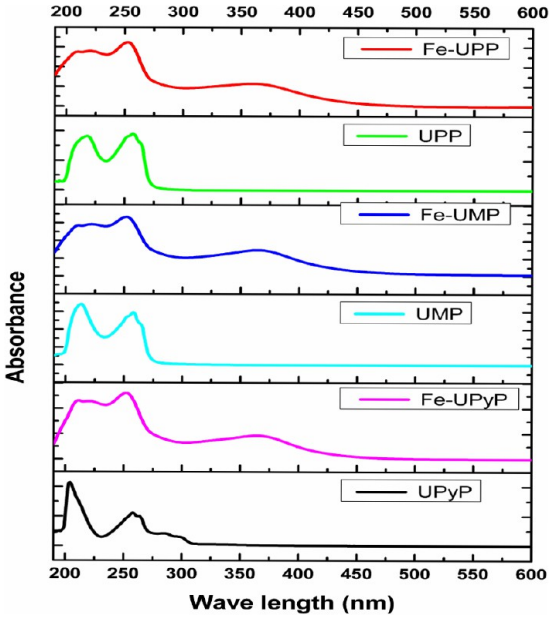

Figure 12. UV−visible adsorption spectrum of free inhibitors (UPyP, UMP, and UPP) and scraped samples (Fe-UPyP, Fe-UMP, and Fe-UPP).

Table 7. UV−Visible Adsorptions of Free Inhibitors and Adsorbed Inhibitors Scraped from a Mild Steel Surface

compounds	$\pi \rightarrow \pi^*$ transition (nm)	n $\rightarrow \pi^*$ transition (nm)	new n $\rightarrow \pi^*$ transition (nm)
UPyp	207	258	-
Fe-UPyP	212	252	363
UMP	213	258	-
Fe-UMP	222	252	364
UPP	217	256	-
Fe-UPP	219	253	360

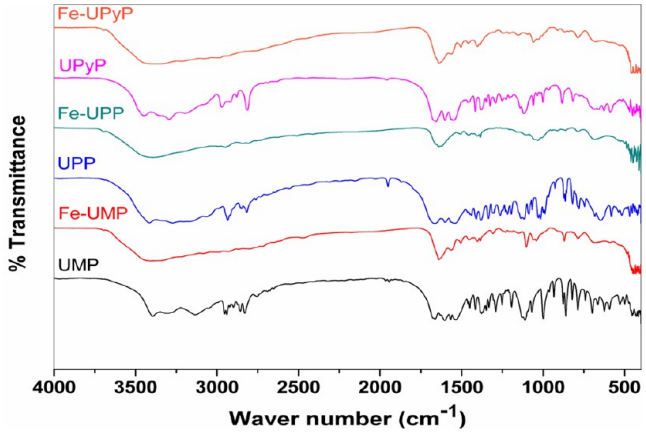

Figure 13. FT-IR adsorption spectrum of free inhibitors (UMP, UPP, and UPyP) and scraped samples Fe-UMP, Fe-UPP, and Fe-UPyP.

presence of different concentrations of synthesized inhibitors (UPyP, UMP, and UPP) was investigated by EIS at 305 K after immersion in acid media for 30 min. Figure 9 shows typical Nyquist and Bode plots were obtained for mild steel in uninhibited and inhibited acidic solutions containing different concentrations of inhibitor molecules. The equivalent circuit model used for the simulation of Nyquist and Bode plots is presented in Figure 10. Inspection of Nyquist plots reveals that the diameter of the reduced semicircle (R_{CT}) increases with an increase in the concentration of studied inhibitors, which is an indication of the inhibition of mild steel corrosion by controlling the charge transfer process.[2] Earlier studies of M. Özcan et al. and Ali Döner et al. show that the diameter of the Nyquist plot is not only based on resistance of inhibitor film but also on resistance of diffuse layer and resistance of corrosion product formed on the metal surface.[51−53] Hence the magnitude of charge transfer resistance (R_{CT}) corresponds to the sum of resistances due to inhibitor film (R_f), diffused layer (R_d), and accumulation of corrosion product (R_a).

The electrochemical corrosion kinetic parameters R_{CT}, C_{dl}, and f_{max} obtained from the experimental and fitted Nyquist plot are listed and compared in Table 6. The magnitude of R_{CT} increases, while the value of double-layer capacitance (C_{dl}) decreases with the addition of the synthesized Mannich bases which results in an increase in percentage inhibition efficiency. It is obvious that the R_{CT} value increase with increasing inhibitor concentration indicates considerable surface coverage due to the adsorption of the inhibitor on the metal surface without altering the corrosion mechanism.

At the same time the values of C_{dl} decreased with increasing inhibitor concentration, which may be attributed to a decrease in the local dielectric constant and/or an increase in the thickness of the electrical double layer, suggesting the formation of a protective layer on the mild steel surface.[54] From the EIS measurements, it is found that all the Mannich bases are good inhibitors showing more than 92% inhibition efficiency at 200 ppm concentrations.

3.4. Surface Analysis. *3.4.1. Scanning Electron Microscopy.* SEM photographs of the mild steel specimen surface in the absence and presence of inhibitors after the immersion in 1.0 M HCl solution for 2 h are shown in Figure 11. The uninhibited mild steel surface appears very uneven and highly damaged, while the inhibited mild steel has a smooth surface. It reveals that a protective layer of adsorbed inhibitor on the mild steel surface prevents acid attack.

3.4.2. UV−Visible Analysis. The thin solid layer formed on the mild steel specimens after completion of a weight loss experiment was scraped, collected, and subjected to spectral studies. Figure 12 shows the UV−visible spectrum of all the free inhibitors, and scraped samples were recorded in methanol. The UV−visible spectrum in methanol exhibits an absorption band in the region of 252−258 nm which can be assigned to n $\rightarrow \pi^*$ transition of carbonyl group. The absorption band obtained at 207−222 nm can be assigned to $\pi \rightarrow \pi^*$ transition of carbonyl and aromatic groups.

The scraped corrosion products exhibit additional n $\rightarrow \pi^*$ transitions at 360−364 nm confirming inhibitor−metal surface interactions. Table 7 shows the UV−visible spectral data of both free inhibitors and scraped samples. Comparing the $\pi \rightarrow \pi^*$ transition of the original inhibitors and scraped samples shows a bathochromic shift; at the same time, a hypsochromic shift was observed in the n $\rightarrow \pi^*$ transition. This indicates the presence of an interaction of π-electrons with vacant d-orbitals of the metal and an interaction between unshared electron pairs in the inhibitor molecule and vacant d-orbitals of the metal, respectively.

3.4.3. FT-IR Analysis. The FT-IR spectra were recorded for free inhibitors (UPyP, UMP, and UPP) and scraped samples Fe-UPyP, Fe-UMP, and Fe-UPP. Figure 13 shows all the characteristic bands corresponding to the functional groups present in the FT-IR spectra of free inhibitors and scraped

DOI: 10.1021/acs.jpcc.5b05788
J. Phys. Chem. C 2015, 119, 22025−22043

Table 8. FT-IR Absorption Frequencies for the Free Inhibitors and the Adsorbed Inhibitors on a Mild Steel Surface

inhibitor UPyP (cm^{-1})	sample Fe-UPyP (cm^{-1})	inhibitor UMP (cm^{-1})	sample Fe-UMP (cm^{-1})	inhibitor UPP (cm^{-1})	sample Fe-UPP (cm^{-1})	tentative assignment
3450, 3295	3387, 3212	3395, 3311	3385, 3219	3414, 3275	3387	ν(N−H)
1657	1639.8	1665	1640	1676, 1654	1641	ν(C═O)
1602	1505	1602	1505	1603	1505	ν(C═C) and ν(C═N) pyridine ring
-	-	1068	1042	-	-	ν(C−O−C) morpholine ring
1140	1152	1130	1150	1151	1162	ν(C−N)
1119	1094	1112	1103	1114	1096	new ν(C−N)
775	786	787	786	778	783	NH_2 wagging
661	668	646	668	655	680	C═O deformation
-	525	-	524	-	517	ν(Fe−O)
-	480	-	474	-	480	ν(Fe−N)

Table 9. Entire Calculated Attributes of UPyP, UMP, and UPP Mannich Base Inhibitors

inhibitor	E_{HOMO} (eV)	E_{LUMO} (eV)	ΔE (eV)	μ	η	IP (eV)	EA (eV)	ω	ΔN	dipole moment (Debye)
UPyP	−5.8200	−0.4963	5.3236	−3.1581	2.6618	5.8200	0.4963	1.8734	0.7216	4.5988
UMP	−5.6480	−0.8174	4.8306	−3.2327	2.4153	5.6480	0.8174	2.1633	0.7798	3.3251
UPP	−5.9049	−0.5001	5.4048	−3.2025	2.7024	5.9049	0.5001	1.8975	0.7026	4.9804

samples. The structurally important IR absorption frequencies of scraped samples along with those of the free inhibitors are compared in Table 8. The stretching frequency due to C═O in inhibitors was shifted to lower frequency in the inhibitor molecules adsorbed onto the mild steel surface, revealing that the unshared pair of electrons on carbonyl oxygen are strongly interacting with the vacant d-orbitals of the metal surface. Consequently the C−N peaks are shifted to higher frequency in the inhibitors adsorbed onto the metal surface. In addition the N−H band is shifted to lower frequency due to the presence of electrostatic interaction between protonated inhibitor molecules and corrosion sites present in the metal surface. The characteristic band due to aromatic C═C was shifted to lower frequency in scraped samples. This indicates that π-electrons of the pyridine ring strongly interact with the vacant d-orbitals of the metal surface. The absorption band due to C−O−C stretching frequency present in inhibitor UMP (shifted from 1068 to 1042 cm^{-1}) indicates an oxygen atom present in the morpholine ring also contributes to the adsorption process.

This may be attributed to additional inhibition efficiency of UMP. The inhibitor molecules adsorbed on the steel surface showed shifts in the C═O, C−N, N−H, and C═C stretching bands, indicating that the inhibitors were adsorbed on the mild steel either via chemisorption, physisorption, or both mechanisms.

3.5. Quantum Chemical Calculations. In general, the E_{HOMO} is associated with electron-releasing ability of the molecule. The higher value of E_{HOMO} denotes the nature of more electron-donating ability. A lower value in E_{LUMO} indicates the nature of the electron-accepting ability of the molecule from the donor sites.[14,55,56] For a better inhibitor molecule, it should contain higher E_{HOMO} to contribute the electrons toward the unoccupied d-orbital of the metal and lower E_{LUMO} value to accept the electrons transferred from the metal surface, and the energy gap ΔE must be least. The present analysis indicates that UMP has excellent inhibition property due to a lower ΔE value of 4.8306 eV than the other two. The ΔE value for UPyP and UPP is 5.3236 and 5.4048 eV, respectively, and all the attributes are given in Table 9. The optimized geometry and HOMO and LUMO pictorial representation of all three inhibitors are given in the Figure 14.

To understand the participation of every individual atom of an inhibitor, HOMO and LUMO are evaluated using the QMForge Software tool.[57] Every individual inhibitor is fragmented into three segments, namely, F−I, F−II, and F−III. The partaking of each fragment and their HOMO and LUMO percentage contributions were given in Table 10. In UPyP, 77% of HOMO is significantly contributed by the pyrrolidine residue (F−II), and 78% of LUMO shifted toward the 4-methylpyridine ring residue (F−I). In the case of UMP, 83% of HOMO localized at the morpholine residue (F−II) promotes contribution of the electron toward metal, and 85% of LUMO formed on the 4-methylpyridine ring residue (F−I) favors receiving the electron cloud from a donor site and can delocalize the electrons of the metal. With respect to UPP, 79% of HOMO formed at the piperidine residue (F−II), and 82% of LUMO formed on the 4-methylpyridine ring (F−I) residue.

Earlier studies of F. Bentiss et al. clearly show that the presence of the heteroatom in the inhibitor molecular system with an unshared pair of electrons such as N, O, and S, etc. can form a coordination bond with the vacant d-orbital of iron.[58] The same trend is observed in UMP. The sum of total negative charges on all heteroatoms (N, O) is higher in UMP than the other two by −3.0606e. A computational report on Mulliken charges is presented in Table 11. Therefore, Mulliken charge analysis fortifies better inhibition property of UMP. The visualization of charge distribution provided by a electrostatic potential (ESP) map is given in Figure 14. The net heteroatom charge for UPyP is −2.5549e and −2.5539e for UPP.

The dipole moment is another important property, which has much influence on determining the inhibition nature of the molecule upon the metal surface.[11] In general, the dipole moment is reciprocally related to inhibition efficiency.[40] Our present study indicates that the UMP has the least calculated dipole moment compared to the other two, which again confirms the superiority of UMP on inhibition out of the remaining two. The dipole moment value for UPyP and UPP is 4.5988 and 4.9804 D correspondingly.

The ΔN has an intimate relationship with the adsorption phenomenon. The mathematical representation of ΔN is provided in eq 12. Here, χ_{Fe} and χ_{inh} denote absolute electronegativity of iron and the inhibitor, respectively. The η_{Fe}

DOI: 10.1021/acs.jpcc.5b05788
J. Phys. Chem. C 2015, 119, 22025−22043

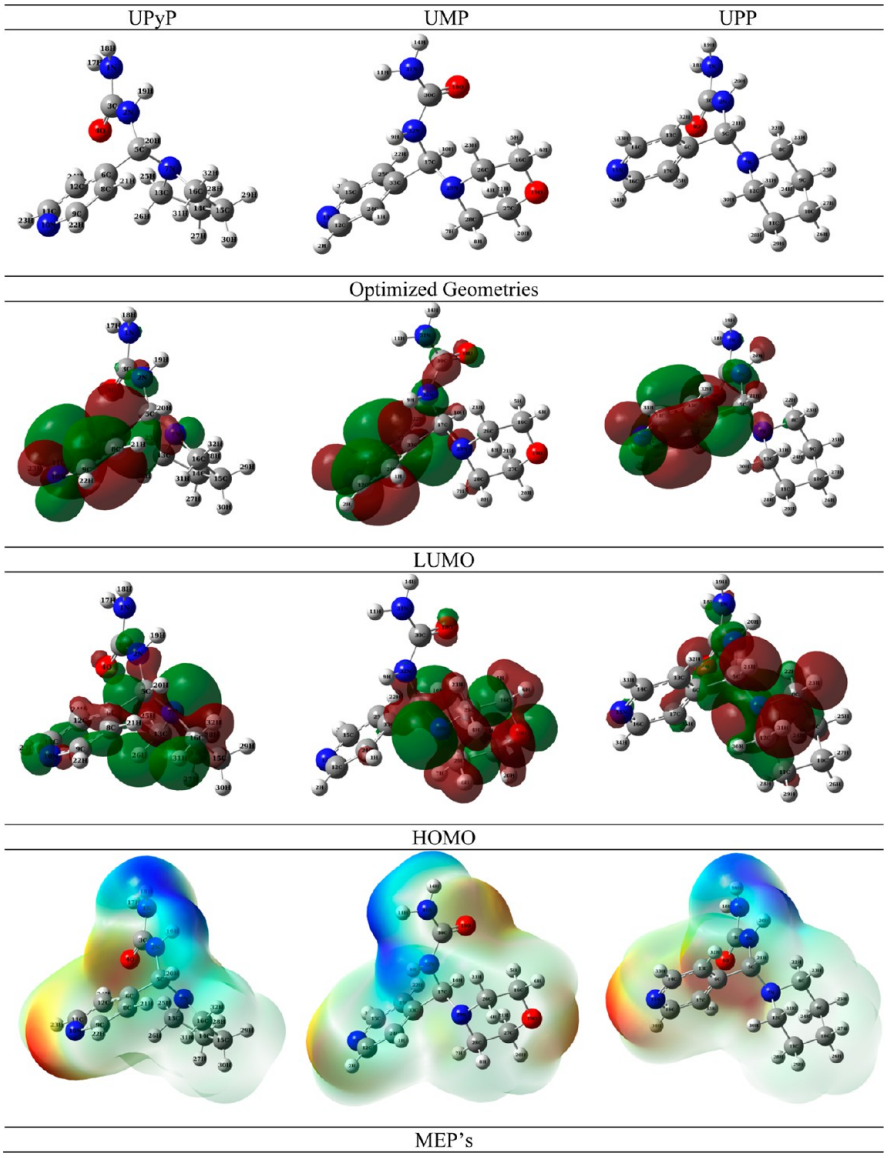

Figure 14. Optimized geometry, HOMO, LUMO, and MEP of UPyP, UMP, and UPP Mannich base inhibitors.

and η_{inh} represent the absolute hardness of iron and the inhibitor molecule, respectively. These two attributes are derived from electron affinity (EA) and ionization potential (IP) quantities.[3] The χ value calculated theoretically for iron metal is 7 eV mol^{-1}, and the η value is 0 eV mol^{-1}. These values are appropriately substituted to calculate the fraction of transfer of electrons (ΔN).[3] In harmony with Lukovit's study,[45] if the value of ΔN is less than 3.6 then the inhibitor's inhibition efficiency gradually increases with electron-contributing ability on the iron surface. Lukovit's observations considerably coincide with the current scenario. The ΔN value of UMP is 0.7798, which is comparatively higher than the remaining two inhibitors.

The chemical hardness (η) indicates the resistivity of the inhibitor for the physical adsorption process.[40] The η value of UMP is 2.4153. It is lower than the η value of UPyP and UPP. The similar trend is recognized in IP as well. Though other chemical properties such as electronic chemical potential (μ), electron affinity (EA), and global electrophilicity index (ω) are closely inter-related, a derived direct relevant trend is unnoticed on UPyP, UMP, and UPP.[59] Finally, the computed quantum chemical information paves the way to choose UMP as a better inhibitor than the other two against anticorrosion treatment. Although all the target molecules show significant anticorrosion activity, their increasing order of inhibition performance can be given as UPP < UPyP < UMP for the Mannich systems under study.

3.6. Mechanism of Inhibition. The mechanism of inhibition action can be explained on the basis of mode of adsorption. In general the charge on the metal surface, type of interaction with the metal surface, and chemical structure of inhibitor influence the adsorption phenomenon. All the Mannich bases have electronegative donor atoms N, O and π-electrons of the aromatic ring.

These electronegative donor atoms or π-electrons of the aromatic ring or both of them cause efficient adsorption of inhibitors onto the mild steel surface. In HCl solution nitrogen-containing compounds exist as protonated species. Due to having a smaller degree of hydration, chloride ions adsorb at the electrode/solution interface, create an excess negative charge in the vicinity of the electrode/solution interface, and favor more adsorption of the positively charged protonated inhibitors.[48] Hence the protonated inhibitors have a tendency to adsorb onto

DOI: 10.1021/acs.jpcc.5b05788
J. Phys. Chem. C 2015, 119, 22025−22043

Table 10. Frontier Molecular Orbital Energy Level Diagram of UPyP, UMP, and UPP

Inhibitor	Fragments	Contributing Moieties	% of HOMO by Fragments	% of LUMO by Fragments
UPyP	F-I	4-Methyl pyridine	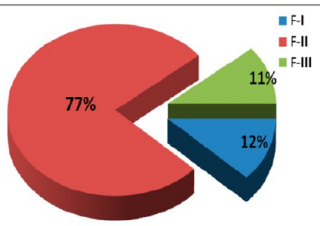	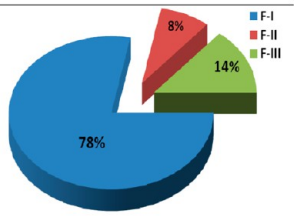
	F-II	Pyrrolidine		
	F-III	Urea		
UMP	F-I	4-Methyl pyridine	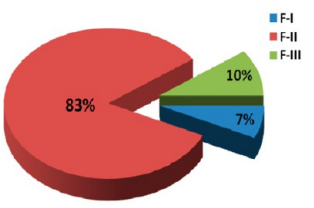	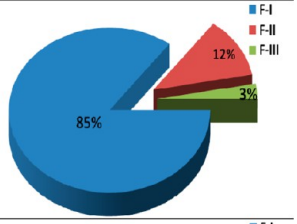
	F-II	Morpholine		
	F-III	Urea		
UPP	F-I	4-Methyl pyridine	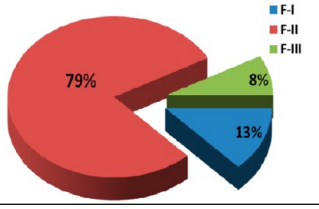	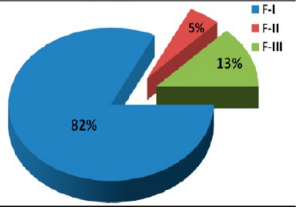
	F-II	Piperidine		
	F-III	Urea		

Table 11. Mulliken Atomic Charges of Heteroatoms in UPyP, UMP, and UPP

inhibitor	Mulliken charges					
UPyP	−0.6300 (N1)	−0.5423 (N2)	−0.4264 (N7)	−0.4324 (N10)	−0.5236 (O4)	-
UMP	−0.4295 (N13)	−0.4480 (N29)	−0.6376 (N31)	−0.5423 (N32)	−0.5187 (O18)	−0.4845 (O19)
UPP	−0.6362 (N1)	−0.5699 (N2)	−0.4204 (N7)	−0.4295 (N15)	−0.4979 (O4)	-

the metal surface through electrostatic interaction between the positively charged molecules and the negatively charged metal surface, thus facilitating physical adsorption of the inhibitors.

In addition to the physical adsorption, the neutral inhibitors may be adsorbed on the mild steel surface through chemical adsorption which can occur through direct sharing of electrons on the basis of donor−acceptor interaction between the π-electrons of the heterocyclic ring and the vacant d-orbital of surface iron atoms.[57] Generally iron has a coordination tendency toward heteroatoms of inhibitor and hence formation of adsorptive film. The formations of adsorptive film on corroding sites of steel through physical or chemical adsorption or through both of them cause reduction of corrosion rate. As inhibitor concentration increases, it covers more and more surface area and results in higher inhibition efficiency. The schematic illustration of different modes of adsorption on the metal/acid interface is shown in Figure 15.

The inhibition efficiency values of the investigated inhibitors for corrosion of mild steel in 1.0 M HCl solution and at different temperatures are in the following order: UMP > UPyP > UPP. One urea moiety and one pyridinyl ring are common in the structure of all three Mannich bases. In addition, UPyP, UMP, and UPP contain pyrrolidino, morpholino and piperidino ring, respectively. The better inhibition performance of UMP than UPyP and UPP is due to the presence of one extra electronegative donor atom O present in the morpholino ring residue involved in a nonbonding interaction with an iron atom.

4. CONCLUSIONS

In the present study, the interactions between three Mannich base inhibitors and mild steel surface have been systematically investigated by weight loss, potentiodynamic polarization, EIS measurements, and DFT calculations.

All the Mannich bases show excellent inhibition properties for the corrosion of mild steel in 1.0 M HCl solutions at different temperatures, and the inhibition efficiency increases with increasing concentration of the inhibitors. The inhibition efficiency measured through weight loss, potentiodynamic polarization, and EIS methods is mutually in good agreement. Tafel polarization measurements show that all the Mannich bases are mixed-type inhibitors with predominant control of the anodic reaction. The values of E_a and ΔH^*_{corr} enhance with the inhibitor concentration, which suggests that the energy barrier of corrosion reaction increases with the presence of Mannich base inhibitors. The adsorption of all studied Mannich bases on the mild steel/HCl solution obeys the Langmuir adsorption isotherm. Large values of K_{ads} and higher negative value of ΔG^0_{ads} indicate that the inhibitor is strongly adsorbed on the metal surface; however, the values of K_{ads} decrease with increasing solution temperature, and lesser negative values of ΔH^0_{ads} strongly support physisorption. FT-IR and UV−vis spectra show that inhibitive action of Mannich bases follows both physisorption and chemisorption mechanisms. SEM micrographs showed that the inhibitor molecules form a good protective film on the mild steel surface. The DFT calculations further confirm the formation adsorptive film through electronegative donor atoms N, O and π-electrons of the pyridinyl ring.

DOI: 10.1021/acs.jpcc.5b05788
J. Phys. Chem. C 2015, 119, 22025−22043

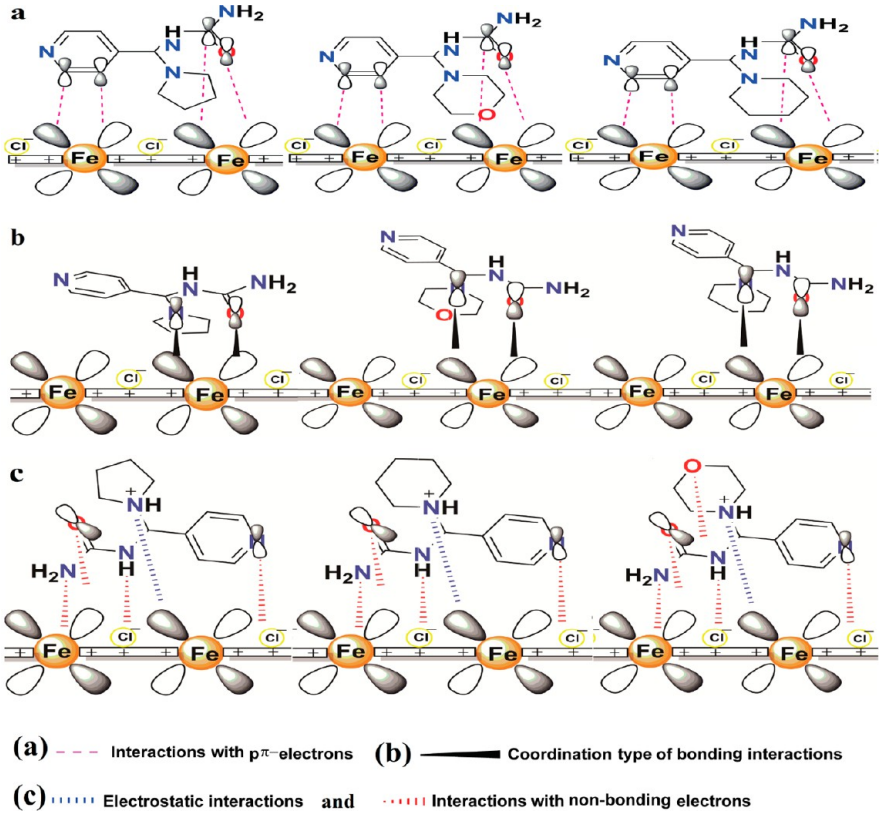

Figure 15. Schematic illustration of different modes of adsorption on the mild steel/1.0 M HCl interface.

The better inhibition efficiency of all the Mannich bases can be explained on the basis of the quantum parameters of E_{HOMO}, E_{LUMO}, ΔE, μ, η, and ΔN. The theoretical calculations are in good agreement with the experimental results, and the inhibition efficiency was found to follow the order UMP > UPyP > UPP.

■ ASSOCIATED CONTENT

Supporting Information

The Supporting Information is available free of charge on the ACS Publications website at DOI: 10.1021/acs.jpcc.5b05788.

^{1}H NMR, ^{13}C NMR, and mass spectrum with fragmentation pattern for all three compounds (PDF)
Crystallographic data for UMP (CIF)
Crystallographic details for UMP (PDF)
Crystallographic data for UPP (CIF)
Crystallographic details for UPP (PDF)

■ AUTHOR INFORMATION

Corresponding Author

*E-mail: venkates@nitt.edu. Tel.: +91 431 2503635. Fax: +91 431 2500133.

Notes

The authors declare no competing financial interest.

■ ACKNOWLEDGMENTS

The first author wishes to acknowledge MHRD, Government of India, for a research fellowship, Department of Chemistry, Indian Institute of Technology, Guwahati, India for the single-crystal XRD analysis, Central drug Research Institute, Lucknow, India, for recording the NMR and Mass spectrum, CARE, Tiruchirappalli, Tamilnadu, India, for SEM analysis, and Sophisticated Test and Instrumentation Centre, Cochin University, Kerala, India, for Elemental analysis.

■ REFERENCES

(1) Ahamad, I.; Prasad, R.; Quraishi, M. A. Inhibition of Mild Steel Corrosion in Acid Solution by Pheniramine Drug: Experimental and Theoretical Study. *Corros. Sci.* **2010**, *52*, 3033−3041.
(2) Gopiraman, M.; Selvakumaran, N.; Kesavan, D.; Kim, I. S.; Karvembu, R. Chemical and Physical Interactions of 1-Benzoyl-3,3-Disubstituted Thiourea Derivatives on Mild Steel Surface: Corrosion Inhibition in Acidic Media. *Ind. Eng. Chem. Res.* **2012**, *51*, 7910−7922.
(3) Ekanem, U. F.; Umoren, S. A.; Udousoro, I. I.; Udoh, A. P. Inhibition of Mild Steel Corrosion in HCl Using Pineapple Leaves-(Ananas Comosus L.) Extract. *J. Mater. Sci.* **2010**, *45*, 5558−5566.
(4) Amin, M. A.; Khaled, K. F.; Mohsen, Q.; Arida, H. A. A Study of the Inhibition of Iron Corrosion in HCl Solutions by Some Amino Acids. *Corros. Sci.* **2010**, *52*, 1684−1695.
(5) Döner, A.; Solmaz, R.; Özcan, M.; Kardas, G. Experimental and Theoretical Studies of Thiazoles as Corrosion Inhibitors for Mild Steel in Sulphuric Acid Solution. *Corros. Sci.* **2011**, *53*, 2902−2913.
(6) Dandia, A.; Gupta, S. L.; Quraishi, M. A.; Singh, P. Ultrasound Assisted Synthesis of Pyrazolo[3,4-b]pyridines as Potential Corrosion Inhibitors for Mild Steel in 1.0 M HCl. *ACS Sustainable Chem. Eng.* **2013**, *1*, 1303.
(7) Sastri, V. S. *Green Corrosion Inhibitors: Theory and Practice*; John Wiley & Sons, Inc.: Hoboken, NJ, 2011.
(8) Manahan, S. E. *Environmental Chemistry*; CRC Press: New York, USA, 1994.
(9) Yadav, D. K.; Quraishi, M. A. Electrochemical Investigation of Substituted Pyranopyrazoles Adsorption on Mild Steel in Acid Solution. *Ind. Eng. Chem. Res.* **2012**, *51*, 8194−8210.
(10) Gopi, D.; Sherif, E. M.; Manivannan, V.; Surendiran, M.; Kavitha, L. Corrosion and Corrosion Inhibition of Mild Steel in Groundwater at Different Temperatures by Newly Synthesized Benzotriazole and Phosphono Derivatives. *Ind. Eng. Chem. Res.* **2014**, *53*, 4286−4294.

DOI: 10.1021/acs.jpcc.5b05788
J. Phys. Chem. C 2015, 119, 22025−22043

(11) Kovačević, N.; Kokalj, A. DFT Study of Interaction of Azoles with Cu(111) and Al(111) Surfaces: Role of Azole Nitrogen Atoms and Dipole-Dipole Interactions. *J. Phys. Chem. C* **2011**, *115*, 24189−24197.
(12) Achary, G.; Sachin, H. P.; Naik, Y. A.; Venkatesha, T. V. The Corrosion Inhibition of Mild Steel by 3-formyl-8-hydroxy Quinoline in Hydrochloric Acid Medium. *Mater. Chem. Phys.* **2008**, *107*, 44−50.
(13) Karthik, D.; Tamilvendan, D.; Prabhu, G. V. Study on the Inhibition of Mild Steel Corrosion by 1,3-bis-(morpholin-4-yl-phenyl-methyl)-thiourea in Hydrochloric Acid Medium. *J. Saudi Chem. Soc.* **2014**, *18*, 835.
(14) Ahamad, I.; Prasad, R.; Quraishi, M. A. Adsorption and Inhibitive Properties of Some New Mannich Bases of Isatin Derivatives on Corrosion of Mild Steel in Acidic Media. *Corros. Sci.* **2010**, *52*, 1472−1481.
(15) Singh, A. K.; Quraishi, M. A. Inhibiting Effects of 5-substituted Isatin-Based Mannich Bases on the Corrosion of Mild Steel in Hydrochloric Acid Solution. *J. Appl. Electrochem.* **2010**, *40*, 1293−1306.
(16) Yadav, M.; Sharma, U.; Yadav, P. N. Isatin Compounds as Corrosion Inhibitors for N80 Steel in 15% HCl. *Egypt. J. Pet.* **2013**, *22*, 335−344.
(17) Thiraviyam, P.; Kannan, K. A Study of Synthesized Mannich Base Inhibition on Mild Steel Corrosion in Acid Medium. *J. Iran. Chem. Soc.* **2012**, *9*, 911−921.
(18) Turcio-Ortega, D.; Pandiyan, T.; Cruz, J.; Garcia-Ochoa, E. Interaction of Imidazoline Compounds with Fe_n (n = 1−4 Atoms) as a Model for Corrosion Inhibition: DFT and Electrochemical Studies. *J. Phys. Chem. C* **2007**, *111*, 9853−9866.
(19) Hosseini, M. G.; Khalilpur, H.; Ershad, S.; Saghatforoush, L. Protection of Mild Steel Corrosion with new Thia-Derivative Salens in 0.5 M H_2SO_4 Solution. *J. Appl. Electrochem.* **2010**, *40*, 215−223.
(20) Emregül, K. C.; Atakol, O. Corrosion Inhibition of Iron in 1 M HCl Solution with Schiff Base Compounds and Derivatives. *Mater. Chem. Phys.* **2004**, *83*, 373−379.
(21) Tamilvendan, D.; Rajeswari, S.; Ilavenil, S.; Chakkaravarthy, K.; Prabhu, G. V. Syntheses, Spectral, Crystallographic, Antimicrobial, and Antioxidant Studies of Few Mannich Bases. *Med. Chem. Res.* **2012**, *21*, 4129−4138.
(22) Pandeya, S. N.; Sriram, D.; Nath, G.; DeClercq, E. Synthesis, Antibacterial, Antifungal and Anti-HIV Activities of Schiff and Mannich Bases Derived from Isatin Derivatives and N-[4-(49-chlorophenyl)-thiazol-2-yl] thiosemicarbazide. *Eur. J. Pharm. Sci.* **1999**, *9*, 25−31.
(23) Ali, M. A.; Shaharyar, M. Oxadiazole Mannich Bases: Synthesis and Antimycobacterial Activity. *Bioorg. Med. Chem. Lett.* **2007**, *17*, 3314−3316.
(24) Tramontini, M.; Angiolini, L. *Mannich Bases: Chemistry and Uses*; CRC Press: London, Tokyo, 1994.
(25) Khaled, K. F. Adsorption and Inhibitive Properties of a New Synthesized Guanidine Derivative on Corrosion of Copper in 0.5 M H_2SO_4. *Appl. Surf. Sci.* **2008**, *255*, 1811−1818.
(26) Oguzie, E. E.; Adindu, C. B.; Enenebeaku, C. K.; Ogukwe, C. E.; Chidiebere, M. A.; Oguzie, K. L. Natural Products for Materials Protection: Mechanism of Corrosion Inhibition of Mild Steel by Acid Extracts of Piper guineense. *J. Phys. Chem. C* **2012**, *116*, 13603−13615.
(27) Kokalj, A.; Peljhan, S. Density Functional Theory Study of ATA, BTAH, and BTAOH as Copper Corrosion Inhibitors: Adsorption onto Cu(111) from Gas Phase. *Langmuir* **2010**, *26*, 14582−14593.
(28) Yadav, M.; Kumar, S.; Sinha, R. R.; Behera, D. Experimental and Quantum Chemical Studies on Corrosion Inhibition Performance of Benzimidazole Derivatives for Mild Steel in HCl. *Ind. Eng. Chem. Res.* **2013**, *52*, 6318.
(29) Gholami, M.; Danaee, I.; Maddahy, M. H.; RashvandAvei, M. Correlated ab Initio and Electroanalytical Study on Inhibition Behavior of 2-Mercaptobenzothiazole and Its Thiole−Thione Tautomerism Effect for the Corrosion of Steel (API 5L X52) in Sulphuric Acid Solution. *Ind. Eng. Chem. Res.* **2013**, *52*, 14875−14889.
(30) Fu, J. J.; Li, S. N.; Wang, Y.; Cao, L. H.; Lu, L. D. Computational and Electrochemical Studies of Some Amino Acid Compounds as Corrosion Inhibitors for Mild Steel in Hydrochloric Acid Solution. *J. Mater. Sci.* **2010**, *45*, 6255−6265.
(31) Pan, Y. C.; Wen, Y.; Xue, L. Y.; Guo, X. Y.; Yang, H. F. Adsorption Behavior of Methimazole Monolayers on a Copper Surface and Its Corrosion Inhibition. *J. Phys. Chem. C* **2012**, *116*, 3532−3538.
(32) Rajeswari, S.; Prabhu, G. V.; Tamilvendan, D.; Ramkumar, V. Spectroscopic Studies and Crystal Structure of 1-(Morpholino(Phenyl) Methyl) Pyrrolidine-2,5-Dione. *J. Chem. Crystallogr.* **2010**, *40*, 437−442.
(33) Pandeya, S. N.; Sriram, D.; Nath, G.; Clercq, E. D. Synthesis, Antibacterial, Antifungal and Anti-HIV Evaluation of Schiff and Mannich Bases of Isatin Derivatives with 3-Amino-2-methylmercapto quinazolin-4(3H)-one. *Pharm. Acta Helv.* **1999**, *74*, 11−17.
(34) Idhayadhulla, I.; Kumar, R. S.; Nasser, A. J. A.; Manilal, J. S. A. Synthesis of Some Mannich Base Derivatives and Their Antimicrobial Activity Study. *Arabian J. Chem.* **2014**, *7*, 994.
(35) *Bruker SHELXTL*. Version 5.1 (includes XS, XL, XP, XSHELL); Bruker AXS Inc.: Madison, Wisconsin, USA, 1999.
(36) Farrugia, L. J. WinGX Suite for Small-Molecule Single-Crystal Crystallography. *J. Appl. Crystallogr.* **1999**, *32*, 837−838.
(37) Farrugia, L. J. ORTEP-3 for Windows - a Version of ORTEP-III with a Graphical User Interface (GUI). *J. Appl. Crystallogr.* **1997**, *30*, 565.
(38) Kumar, S. L. A.; Gopiraman, M.; Kumar, M. S.; Sreekanth, A. 2-Acetylpyridine-N(4)-Morpholine Thiosemicarbazone (HAcpMTSc) as a Corrosion Inhibitor on Mild Steel in HCl. *Ind. Eng. Chem. Res.* **2011**, *50*, 7824−7832.
(39) Lebrini, M.; Lagrenée, M.; Vezin, H.; Traisnel, M.; Bentiss, F. Experimental and Theoretical Study for Corrosion Inhibition of Mild Steel in Normal Hydrochloric Acid Solution by Some New Macrocyclic Polyether Compounds. *Corros. Sci.* **2007**, *49*, 2254−2269.
(40) John, S.; Joseph, A. Effective Inhibition of Mild Steel Corrosion in 1 M Hydrochloric Acid Using Substituted Triazines: an Experimental and Theoretical Study. *RSC Adv.* **2012**, *2*, 9944−9951.
(41) Parr, R. G.; Yang, W. *Density-Functional Theory of Atoms and Molecules*; Oxford University Press: New York, 1989.
(42) Parr, R. G.; Szentpály, L. V.; Liu, S. Electrophilicity Index. *J. Am. Chem. Soc.* **1999**, *121*, 1922−1924.
(43) Parr, R. G.; Donnelly, R. A.; Levy, M.; Palke, W. E. Electronegativity: The Density Functional Viewpoint. *J. Chem. Phys.* **1978**, *68*, 3801−3807.
(44) Sanderson, R. T. Electronegativity and Bond Energy. *J. Am. Chem. Soc.* **1983**, *105*, 2259−2261.
(45) Lukovits, I.; Kálmán, E.; Zucchi, F. Corrosion Inhibitors-Correlation Between Electronic Structure and Efficiency. *Corrosion* **2001**, *57*, 3−8.
(46) Frisch, M. J.; Trucks, G. W.; Schlegel, H. B.; Scuseria, G. E.; Robb, M. A.; Cheeseman, J. R.; Montgomery, J. A.; Vreven, Jr., T.; Kudin, K. N.; Burant, J. C.; et al. *Gaussian 03*; Gaussian Inc.: Pittsburgh PA, 2003.
(47) Quraishi, M. A.; Singh, A.; Singh, V. K.; Yadav, D. K.; Singh, A. K. Green Approach to Corrosion Inhibition of Mild Steel in Hydrochloric Acid and Sulphuric Acid Solutions by the Extract of Murraya Koenigii Leaves. *Mater. Chem. Phys.* **2010**, *122*, 114−122.
(48) Ahmad, Z. *Principles of Corrosion Engineering and Corrosion Control*; Elsevier Science & Technology Books: New York, 2006.
(49) Gomma, G. K. Corrosion inhibition of Steel by Benzotriazole in Sulphuric Acid. *Mater. Chem. Phys.* **1998**, *55*, 235−240.
(50) Martinez, S.; Stern, I. Thermodynamic Characterization of Metal Dissolution and Inhibitor Adsorption Processes in the Low Carbon Steel/Mimosa Tannin/Sulfuric Acid System. *Appl. Surf. Sci.* **2002**, *199*, 83−89.
(51) Özcan, M.; Dehri, İ.; Erbil, M. Organic Sulphur-Containing Compounds as Corrosion Inhibitors for Mild Steel in Acidic media: Correlation between Inhibition Efficiency and Chemical Structure. *Appl. Surf. Sci.* **2004**, *236*, 155−164.
(52) Döner, A.; Kardas, G. N-Aminorhodanine as an Effective Corrosion Inhibitor for Mild Steel in 0.5 M H2SO4. *Corros. Sci.* **2011**, *53*, 4223−4232.
(53) Yıldız, R.; Döner, A.; Doğan, T.; Dehri, İ. Experimental Studies of 2-pyridinecarbonitrile as Corrosion Inhibitor for Mild Steel in Hydrochloric Acid Solution. *Corros. Sci.* **2014**, *82*, 125−132.

DOI: 10.1021/acs.jpcc.5b05788
J. Phys. Chem. C 2015, 119, 22025−22043

(54) Benabdellah, M.; Tounsi, A.; Khaled, K. F.; Hammouti, B. Thermodynamic, Chemical and Electrochemical Investigations of 2-mercapto benzimidazole as Corrosion Inhibitor for Mild Steel in Hydrochloric Acid Solutions. *Arabian J. Chem.* **2011**, *4*, 17−24.
(55) Liu, B. Y.; Liu, Z.; Han, G. C.; Li, Y. H. Corrosion Inhibition and Adsorption Behavior of 2-((dehydroabietylamine)methyl)-6-methoxyphenol on Mild Steel Surface in Seawater. *Thin Solid Films* **2011**, *519*, 7836−7844.
(56) Boobalan, M. S.; Ramalingam, S.; Amaladasan, M.; Tamilvendan, D.; Prabhu, G. V.; Bououdina, M. A Computational Perspective on Equilibrium Geometry, Vibrational Spectra and Electronic Structure of Antioxidant Active Mannich Base 1-[(Pyridin-2-yl amino) methyl] pyrrolidine-2,5-dione. *J. Mol. Struct.* **2014**, *1072*, 153−172.
(57) Tenderholt, A. L. *QMForge*, Version 2.1; Stanford University: Stanford, CA, USA.
(58) Bentiss, F.; Traisnel, M.; Lagrenee, M. The Substituted 1,3,4-oxadiazoles: a New Class of Corrosion Inhibitors of Mild Steel in Acidic Media. *Corros. Sci.* **2000**, *42*, 127−146.
(59) Behpour, M.; Ghoreishi, S. M.; Soltani, N.; Niasari, M. S.; Hamadanian, M.; Gandomi, A. Electrochemical and Theoretical Investigation on the Corrosion Inhibition of Mild Steel by Thiosalicylaldehyde Derivatives in Hydrochloric Acid Solution. *Corros. Sci.* **2008**, *50*, 2172−2181.

DOI: 10.1021/acs.jpcc.5b05788
J. Phys. Chem. C 2015, 119, 22025−22043